ACS OMEGA

http://pubs.acs.org/journal/acsodf

Review

Integration of 3D Printing–Coelectrospinning: Concept Shifting in Biomedical Applications

Adrija Ghosh, Jonathan Tersur Orasugh, Suprakas Sinha Ray,* and Dipankar Chattopadhyay

Cite This: *ACS Omega* 2023, 8, 28002–28025

Read Online

ACCESS | Metrics & More | Article Recommendations

ABSTRACT: Porous structures with sizes between the submicrometer and nanometer scales can be produced using efficient and adaptable electrospinning technology. However, to approximate desirable structures, the construction lacks mechanical sophistication and conformance and requires three-dimensional solitary or multifunctional structures. The diversity of high-performance polymers and blends has enabled the creation of several porous structural conformations for applications in advanced materials science, particularly in biomedicine. Two promising technologies can be combined, such as electrospinning with 3D printing or additive manufacturing, thereby providing a straightforward yet flexible technique for digitally controlled shape-morphing fabrication. The hierarchical integration of configurations is used to imprint complex shapes and patterns onto mesostructured, stimulus-responsive electrospun fabrics. This technique controls the internal stresses caused by the swelling/contraction mismatch in the in-plane and interlayer regions, which, in turn, controls the morphological characteristics of the electrospun membranes. Major innovations in 3D printing, along with additive manufacturing, have led to the production of materials and scaffold systems for tactile and wearable sensors, filtration structures, sensors for structural health monitoring, tissue engineering, biomedical scaffolds, and optical patterning. This review discusses the synergy between 3D printing and electrospinning as a constituent of specific microfabrication methods for quick structural prototypes that are expected to advance into next-generation constructs. Furthermore, individual techniques, their process parameters, and how the fabricated novel structures are applied holistically in the biomedical field have never been discussed in the literature. In summary, this review offers novel insights into the use of electrospinning and 3D printing as well as their integration for cutting-edge applications in the biomedical field.

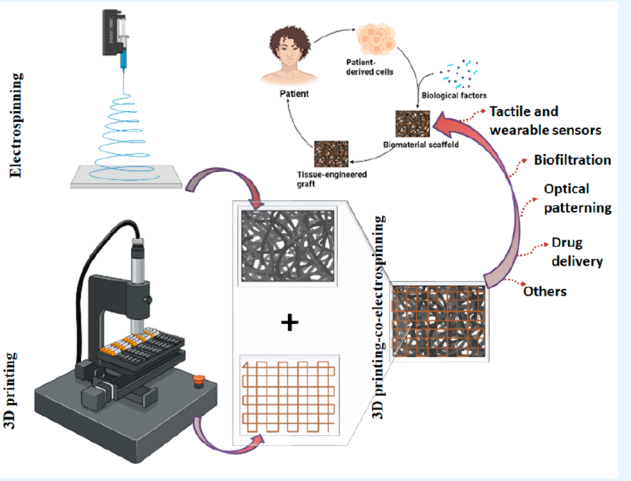

1. INTRODUCTION

Three-dimensional (3D) printing is one of the most effective techniques for developing 3D objects by deposition of source materials, such as polymers or ceramics, in a layered manner.[1] It is also referred to as rapid prototyping (RP), solid free-form technology (SFF), or additive manufacturing (AM).[2,3] In 1981 Dr. Hideo Kodama invented the rapid prototyping machine that could polymerize resin using ultraviolet (UV) light and fabricate parts layer-by-layer.[4] Chuck Hull, the "inventor of 3D printing", filed the first patent for stereolithography in 1986.[5] He created and commercialized selective laser sintering (SLS) and the .stl format (the general file type for 3D printing). SLS, a different type of 3D printer, was first licensed by a student at the University of Texas, Carl Deckard, in 1988.[6] In 1989, fused deposition modeling (FDM) was patented by Scott Crump.[7] He founded Stratasys, which is currently one of the largest manufacturers of 3D printers. In the same year, the SLA-1 3D printer was released by Hull's 3D Systems Corporation. Since the invention of commercial 3D printers, they have been utilized in aerospace, construction, healthcare, and other fields. In addition, manufacturers are attempting to develop materials that are resistant to heat, flames, and chemicals. Cellink, a Swedish company, introduced bioink based on seaweed that can be used for printing biological tissues and human organs.[8]

The use of 3D printing in the biomedical field is growing considerably and is expected to become revolutionary in the healthcare sector. Biomedical applications of 3D printing include the fabrication of tissues and organs,[9] prosthetics,[10]

Received: June 4, 2023
Accepted: July 6, 2023
Published: July 25, 2023

Table 1. 3D-Printed Hydrogels Used in Biomedical Applications

Hydrogel composition	Cross-linker used	3D printing technique used	Applications	ref
Hydroxypropyl methylcellulose	Cross-linking via hydrogen bonding	Semisolid extrusion 3D printer	Extended-release tablets of theophylline	23
Poly(ethylene glycol) dimethacrylate	Ascorbic acid	SLA 3D printer	Successful load and release of ascorbic acid	24
Alginate/bacterial-cellulose/copper hydrogel	Calcium and copper ions	3D bioplotter	Antimicrobial	25
Polyacrylamide/hydroxypropyl methylcellulose	Silver nanoparticles	FDM 3D printer	Wound healing	26
Poly(vinyl alcohol)/graphene oxide/hydroxyapatite	Ionic crystallization cross-linking	Microextrusion 3D printing	Artificial cartilage replacement	27
Chitosan-pectin	Physical cross-linking	Piston-based mechanical dispensing extrusion 3D printer	Wound dressing	28
Hyaluronic acid/alginate	Catechol and calcium ions	Extrusion-based 3D printer	Tissue engineering	29
Alginate dialdehyde/gelatin/silica-calcia nanoparticles	Calcium ions	Extrusion-based 3D printer	Bone tissue engineering	30
Graphene oxide/hydroxyapatite/gelatin	Ionic crystallization cross-linking	3D bioplotter	Orthopedic applications	31
Poly(vinyl alcohol)/chitosan	Ionic crystallization cross-linking	Extrusion-based 3D printer	Biomedical application	32
Silk/gelatin	Horseradish peroxidase mediated enzymatic cross-linking	Extrusion-based 3D printer	Cartilage regeneration	33
Silk/glycidyl-methacrylate	Glycidyl methacrylate	Digital light processing 3D printer	Cartilage regeneration	34

drug delivery,[11] and biosensing.[12] Such applications have various advantages, such as the availability of customized and personalized medicines,[13] medical products, and equipment within budget. Despite these advances, this technique has various scientific and regulatory drawbacks that must be overcome. The integration of 3D printing with another technique, called electrospinning, can overcome these disadvantages.

Electrospinning is a technique aimed at fabricating fibers from a liquid polymeric solution or melt by applying electrostatic forces. Fibers are formed by evaporation of the solvent or freezing of the melt. William Gilbert was the first to observe the behavior of a liquid under the influence of electrostatic force in 1600.[14] John Francis Cooley first patented electrospinning in 1900.[15] In 1964−1969, Sir Geoffrey Ingram Taylor mathematically modeled the shape of the Taylor cone.[16] Since 1995, various research groups have actively worked on electrospun nanofibers and their multiple applications.

As nanofibers with interconnected pores can simulate the structure of a natural extracellular matrix, they are extensively used for biomedical applications, such as tissue regeneration or sustained drug delivery.[17] However, the low mechanical strength of scaffolds or their uncontrollable shapes often limit their use.

The combination of 3D printing and electrospinning yields the benefits of both techniques, essentially producing materials with high porosities, controllable shapes, adequate mechanical strength, and ECM-like properties. Several biocompatible materials have been produced by combining 3D printing and electrospinning. They can also be used in tissue engineering, drug delivery, wearable sensors, and facemasks. This review includes (i) brief insight into the basic working principle, (ii) working parameters, and (iii) biomedical applications of 3D printing and electrospinning. The following sections discuss various combinational strategies and their biomedical applications. Finally, we present the future outlook.

The novelty of this review is that it is the only other review, in addition to that by Yang et al.,[18] available in this regard. However, unlike the aforementioned article by Yang et al.,[18] which focuses primarily only on tissue engineering applications of the combinational approach but does not discuss each technique individually or their process parameters as well as the holistic application of these novel materials in the biomaterial niche, this review discusses them. This review also serves as a foundational support reference for emerging researchers willing to utilize electrospinning or 3D printing as well as their integration for advanced applications.

A comprehensive review of the fundamental principles related to the synergy between 3D printing and electrospinning as a constituent of specific microfabrication for rapid structural prototypes is expected to advance next-generation constructs for biomedical applications.

2. CONVENTIONAL 3D PRINTING

2.1. Biomaterials for 3D Printing. 3D-printed materials intended for biomedical applications are printed using inks composed of biomaterials because they can function as an extracellular matrix, promoting cell support and adherence. Thus, printability, biocompatibility, apposite mechanical strength, nontoxicity, and strong interfacial strength are important features of bioinks for use in the 3D printing of healthcare products. Another crucial criterion for choosing biomaterials is the balance between the degradation and tissue regeneration rates.

Three main groups of biomaterials are typically used for this purpose, as discussed in the following subsections.

2.1.1. Polymeric Hydrogels for 3D Printing. Hydrogels are composed of a porous 3D network produced from cross-linked, man-made hydrophilic biopolymers that can hold high concentrations of water or biological fluids without disintegration, but they will be solubilized. Biocompatible hydrogel inks are widely used for 3D printing because of their ease of extrusion and solidification.[19] Owing to their high moisture content and porosity, they mimic the extracellular matrix (ECM) structure. Additionally, they have the potential to encapsulate bioactive molecules. However, conventionally made hydrogels are fragile and have a low mechanical strength, thereby rendering them inept at mimicking the elasticity of various tissues and maintaining their shapes during printing. Thus, the hydrogels generally used for this application possess

https://doi.org/10.1021/acsomega.3c03920
ACS Omega 2023, 8, 28002−28025

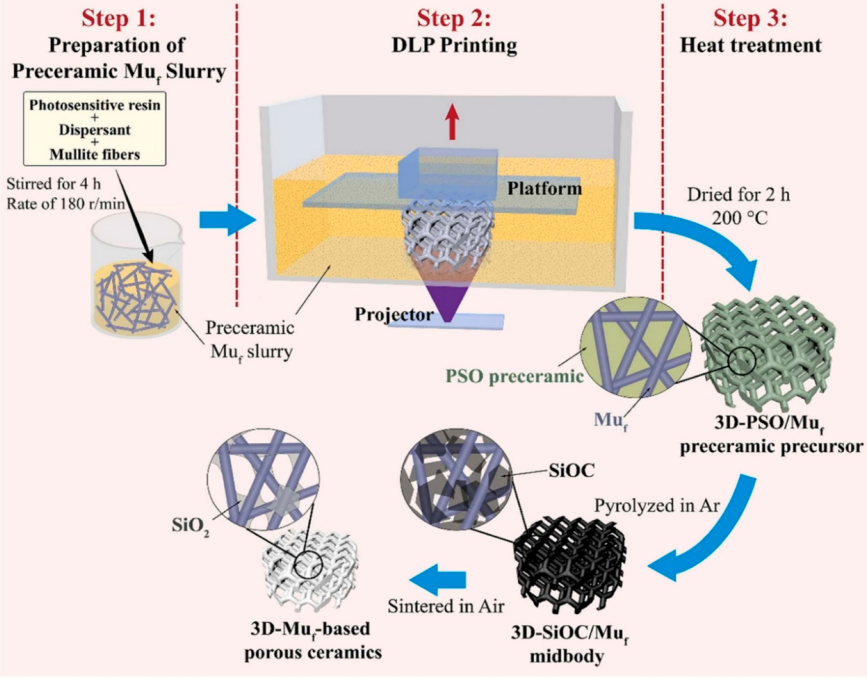

Figure 1. Procedure to fabricate 3D-Mu$_f$-based porous ceramics. Reproduced with permission from Cao et al.[36] Copyright 2022, Elsevier Science Ltd.

high mechanical strength and elasticity. This class of hydrogels includes interpenetrating network (IPN) hydrogels,[20] functionalized single-network hydrogels,[21] and nanocomposite hydrogels.[22]

Hydrogels with an IPN structure generally consist of two interlocked polymeric chains and have much higher mechanical strength compared to individual chains. They can be further classified into semi-IPN and full IPN depending on their structures and synthesis routes. At the same time, nanocomposite hydrogels can be defined as nanoparticle-incorporated hydrogels with enhanced mechanical strength. Nanoparticles can be inorganic, polymeric, or metallic. These nanoparticles were either physically mixed or covalently bonded to the hydrogel's polymeric chains. Conventionally, hydrogels are strengthened by cross-linking or grafting. Sometimes, these hydrogels are double-cross-linked to give them high strength and elasticity. Hydrogels can be cross-linked via multiple ways. For example, hydrogels can be exposed to UV light to generate photoinitiators, which results in the cross-linking of the polymeric chains. However, the effects of these initiators on the cell viability must be considered. The unreacted photoinitiators are cytotoxic. Table 1 lists the different 3D-printed hydrogels used in various biomedical applications.

2.1.2. Thermoplastic Polymers. One of the most widely used polymers for 3D printing purposes is acrylonitrile butadiene styrene (ABS), which is flexible and highly robust. It can endure a wide range of temperatures, from −20 to 80 °C. Another example of a thermoplastic polymer is poly(lactic acid) (PLA), which is widely used in FDM. It is significantly less expensive, can be processed more efficiently, and can be easily synthesized from the feedstock. Additionally, it melts at 175 °C and can be extruded effortlessly in the temperature range of 190−230 °C. Poly(ε-caprolactone) (PCL) is a biodegradable polymer, similar to PLA, and melts at 60 °C. PCL can be easily used in FDM owing to its excellent viscoelasticity and rheological behavior. Another example is polycarbonate (PC), which is highly robust and resistive toward any deformity caused near 150 °C.[19]

2.1.3. Metals. Fe, Co, Cr, stainless steel, and Ti alloys can be used in the fabrication of 3D printing scaffolds. Metals are desirable materials for 3D printing scaffolds owing to their high mechanical strength, which has been demonstrated to be comparable to that of bone. Therefore, they are frequently used for bone tissue regeneration. Metals are intriguing materials because of their strong mechanical stability and, to a lesser extent, their safety when they are used *in vivo*. Several of the aforementioned metals have been used to create traditional scaffolds; however, only a few metals have been employed in 3D printing. These include stainless steel, Co−Cr alloys, Ti and its alloys, and nitinol. Despite being effectively utilized in traditional scaffolding, further research is required to determine the viability of employing certain metals as constituents of 3D-printed scaffolds. However, the two main constraints are (i) the limitations of 3D printing technology, which restrict the types of metals that may be employed, and (ii) the toxicity of metal ions induced by the corrosion of metals and their *in vivo* degradation. A long degradation period is another factor that renders difficulty in employing metals because they cause functional tissues to surround the scaffold rather than eventually replace it.[35]

2.1.4. Ceramic-Based Materials. Ceramics are commonly used as bioink in 3D printing materials for biomedical applications. Ceramic materials, such as hydroxyapatite or calcium phosphate, are highly stiff and have a composition similar to that of bones. These materials have a melting temperature above approximately 2000 °C, and they can be added as additive materials to other polymers for ink in the FDM process.[35] A facile example of ceramic-based 3D printing is depicted in Figure 1.[36] Reportedly, 3D printing coupled SiC chemical vapor infiltration was used by Mei et al.[37] to fabricate structurally controlled 3D porous high-strength ceramics

https://doi.org/10.1021/acsomega.3c03920
ACS Omega 2023, 8, 28002−28025

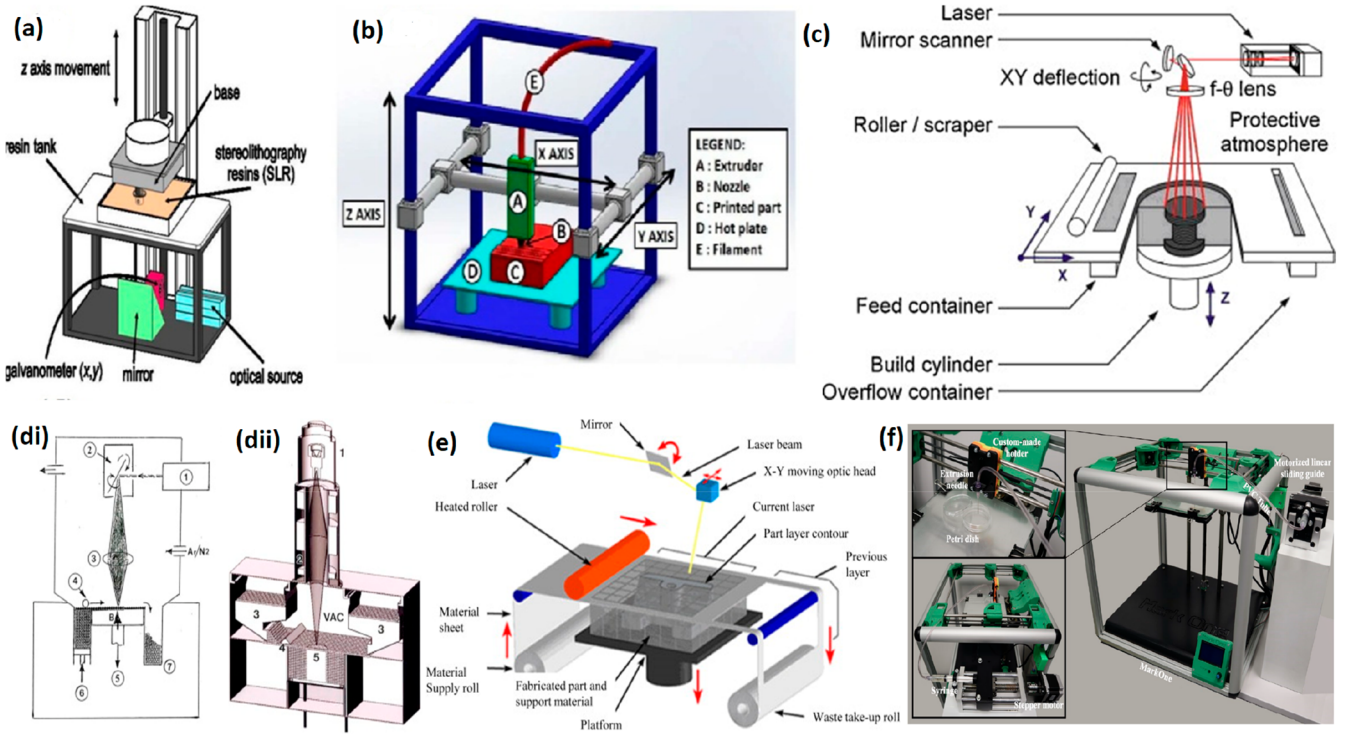

Figure 2. Different parts of an (a) SLA 3D printer and (b) FDM 3D printer. (c) Schematic of the SLS setup. (d) Laser (di) and electron beam (dii) melting systems for powder layer additive manufacturing. (a) Uses an inert atmosphere (N_2 or Ar), whereas (dii) uses a vacuum environment. In (di), laser beam (1) scanning uses a mirror (2) with beam focus at (3); powder is rolled into layers (4) on a build platform (5) from a container at (6) and excess powder is retrieved at (7). In (b), electron gun (1), scanning coils (2), powder cassettes (3), layer rake (4), build table (product) (5). (e) Typical type of LOM process. (f) Final layout of the custom-made 3D bioplotter. Reproduced with permission from Weng et al.,[49] Copyright 2016, Elsevier Science Ltd.; Mazzanti et al.,[61] Copyright 2019, The Authors; Shahzad et al.,[62] Copyright 2014, Elsevier Science Ltd.; Murr,[3] Copyright 2016, Elsevier Science Ltd.; Ahn et al.,[63] Copyright 2012, Elsevier Science Ltd.; and Lovecchio et al.,[64] Copyright 2022, The Authors.

proposed for advanced functional applications, which may also include biomaterials. Liu et al. synthesized scaffolds comprising β-tricalcium phosphate (TCP) using a digital light processing (DLP)-based 3D printer;[38] these scaffolds facilitated cell adhesion and angiogenesis. A ceramic slurry with low viscosity was prepared by blending acrylate resin with β-TCP to obtain a viscosity of 3 Pa s. The scaffolds possessed a maximum compressive strength of 9.89 MPa and a porosity of 40%; additionally, they were highly biocompatible and promoted bone regeneration.

In another report, paste-based extrusion 3D printing was utilized for printing zirconate titanate ceramics to fabricate piezoelectric materials.[39] Yang et al.[40] employed digital light processing 3D printing to fabricate SiC-SiOC ceramics having excellent mechanical properties suitable for diverse advanced applications. Various ceramics, such as ZnO,[41] alumina,[42] $BaTiO_3$,[43] mullite(s) (Figure 1),[36] 3Y-TZP (3 mol % yttria-stabilized tetragonal zirconia),[44] Si_3N_4,[45] ZrO_2 (3Y)/Al_2O_3,[46] SiC_w/Si_3N_4,[47] and Li_4SiO_4,[48] have been utilized for the fabrication of ceramic-based 3D-printed biomaterials.

Regarding the use of ceramics as 3D-printed systems for biomaterial applications, the literature presented earlier has proven that these materials exhibit better mechanical properties, excellent piezoelectric properties similar to those of biological tissues, and excellent support for the proliferation of cultured bone cells.[40]

2.2. Working Principle and Parameters. Various types of 3D printers are available in the market. The next section highlights the working principles and parameters of the most commonly used 3D printers for biomedical applications.

2.2.1. Stereo Lithography (SLA). Compared with other 3D printing methods, SLA is the oldest technique and produces 3D structures with high accuracy and resolution. Figure 2(a) shows different parts of the SLA 3D printer.[49] SLA projects spatially controlled light onto liquid or photopolymerizable bioinks with low viscosity (also referred to as photopolymers) using a particular light source, such as UV, infrared, or visible light and certain optics. SLA uses photopolymerization to solidify a 2D design. This process is initiated by single- or two-photon absorption. Next, through layerwise stacking of two-dimensional designs, 3D structures may be built.[50] However, SLA can employ only photopolymerizable bioinks, and because of their restricted selectivity, bioinks might not be able to sufficiently mimic the conditions needed for cell proliferation and differentiation.

The strength of the SLA product is affected by several variables, among which layer thickness, postcuring period, and orientation contribute the most significantly. In addition, numerous processing factors, including hatch spacing, layer thickness, scan speed, and laser power, affect the accuracy of SLA prototypes.[51] To address this issue, efforts have been made by Kunjan et al.[52] to optimize these process variables for optimum part strength and establish an empirical link between process variables and part strength using the design of experiments. They concluded that the hatch spacing, which accounted for 43.11% of the response's overall variance, had a significant impact on the warpage of the SLA parts. Thus, the

https://doi.org/10.1021/acsomega.3c03920
ACS Omega 2023, 8, 28002−28025

Table 2. Process Parameters for FDM 3D Printing

Parameters	Factors	Influence
Geometrical parameters	Nozzle size	The size of the nozzle diameter varies from 10 to 100 mm. To achieve precision and print speed, 0.4 mm of nozzle size is used in most cases.
	Filament size	Filaments having different properties require different temperatures. Filaments either have a diameter of 1.75 mm or 2.85 mm.
Process parameters	Melting temperature	It can be defined as the temperature of the molten material exiting the extruder.
	Bed temperature	Heated beds are highly required for 3D printing. The apposite range of temperature is between 55 and 70 °C.
	Printing speed	It is one of the most important parameters for 3D printing. It determines the speed of the 3D printer's motor. This includes both extruders along with *X*- and *Y*-axis controlled electric motors.
Structural parameters	Layer thickness	The *Z*-axis' vertical resolution influences the thickness of the layer. All three axes are considered while devising a project using additives.
	Infill geometry	It can be described as a pattern that is infill. These patterns influence printing speed, time, and weight along with the strength and mechanical features of the object. There are four types of patterns.
	Infill density	It can be described as the amount of material filled within the piece, which can be varied between 0 and 100% using rolling programs.
	Raster angle	The angle formed between the *X*-axis of an FDM printer and the nozzle direction can be described as a raster angle. It affects the mechanical properties and shape precision of the printed material. A 90° difference is observed between the raster angles of two successive layers.
	Raster gap	It is the distance of separation between two nearby filaments placed in the same layer.

hatch overcure depth is the most important factor influencing the construction time of SLA parts. The hatch overcure depth has the greatest impact on the upfacing sloped surfaces of the SLA product.

2.2.2. Fused Deposition Modeling (FDM). The FDM technique is based on the principle of heating matter to its melting point, followed by layerwise deposition. In this process, the melted ceramic or polymeric material is extruded via a nozzle with a small orifice that fuses with the deposited material on the layer before it. By mechanically manipulating the $x-y$ direction of the nozzle, the pattern of each layer can be changed, as shown in Figure 2(b).[53] In theory, printing an item with FDM is a rather straightforward process. Counter-rotating gears feed the filament into the printer and force it into the liquefier. Following melting, the feedstock follows a computer-controlled route via a print nozzle before being deposited on a base platform. This procedure is repeated layer-by-layer until the required 3D shape is realized. Multimaterial printing is possible using dual-nozzle printers. Nevertheless, part construction, although appearing simple, is a complicated process controlled by numerous frequently connected factors.[54] The different process parameters that influence the property of 3D-printed products via the FDM process are summarized in Table 2.[55]

2.2.3. Selective Laser Sintering (SLS). This technology carefully utilizes lasers to transform a fine powder bed into a 3D model layer-by-layer. Upon illumination with a high-power laser beam, the powdered particles adhere to each other and solidify; this process is known as sintering. A deflection system controls the scanning laser beam, which is administered by a corresponding cross section computed from a previously designed computer-aided design (CAD) model. The subsequent layer is constructed by depositing and spreading powder onto the formerly deposited layer. This process is repeated until the entire 3D-printed part is developed, as shown in Figure 2(c).[56]

The most significant process parameters for SLS are the hatch spacing, part-bed temperature, laser power, and thickness. As concluded by Whenish et al.,[57] hatch spacing influences surface finish. The space between succeeding layers is large if the hatch spacing is large, which prevents the required bonding strength from being achieved. Scan spacing is the most important variable for both the density and hardness. According to the experimental findings, density and hardness both decrease with increasing scan spacing.[58] Additionally, density and hardness exhibit a relationship with laser power; essentially, they both increase with increasing laser power. Hardness increases continually as the bed temperature increases, whereas the density initially increases and then decreases with an increase in bed temperature. Additionally, the hardness increases as the hatch length increases; however, the density initially decreases and then increases with an increase in hatch length.

2.2.4. Electronic Beam Melting (EBM). This technique involves processing highly reactive materials that melt at high temperatures. An electron beam with a voltage of 30−60 V is used to melt the powders. As EBM is conducted in a highly vacuum environment, challenges, such as oxidation, contamination, and atmospheric intervention, can be avoided. Additionally, EBM has the exceptional feature of building metallic parts from alloyed powder to achieve materials with striking functional and mechanical features, as shown in Figure 2(d).[59] The process parameters involved in the EBM process include beam power, beam scanning velocity, beam focus, beam diameter, beamline spacing, plate temperature, preheated temperature (including the number of repeats, speed, and power of the beam), contour strategies, and scan strategies.

2.2.5. Laminated Object Manufacturing (LOM). In this technique, sheetlike materials are coated with an appropriate adhesive immediately before bonding via a suitable method for effectively bonding the sheet materials. The bonded sheets are consecutively laminated to fabricate the components. A laser beam is used to profile the cut two-dimensionally. Scanning speed and laser power are the most significant process parameters for this technique. To avoid the destruction of the laminated layer, the cutting depth must be equal to the thickness of the layer. A typical LOM process is reported in Figure 2(e).[59] Process parameters that may influence the quality of products fabricated by using the LOM method include laser speed, heater speed, platform retract, platform speed, feeder speed, heater temperature, and layer thickness.

2.2.6. Bioplotter Printing. Bioplotter printing involves the extrusion of thermally or chemically processed materials. Here, the deposition of the material occurs in a layerwise manner, and the composition of each layer may differ. The Bioplotter printer has the ability to use and replace "bioink" in a manner

https://doi.org/10.1021/acsomega.3c03920
ACS Omega 2023, 8, 28002−28025

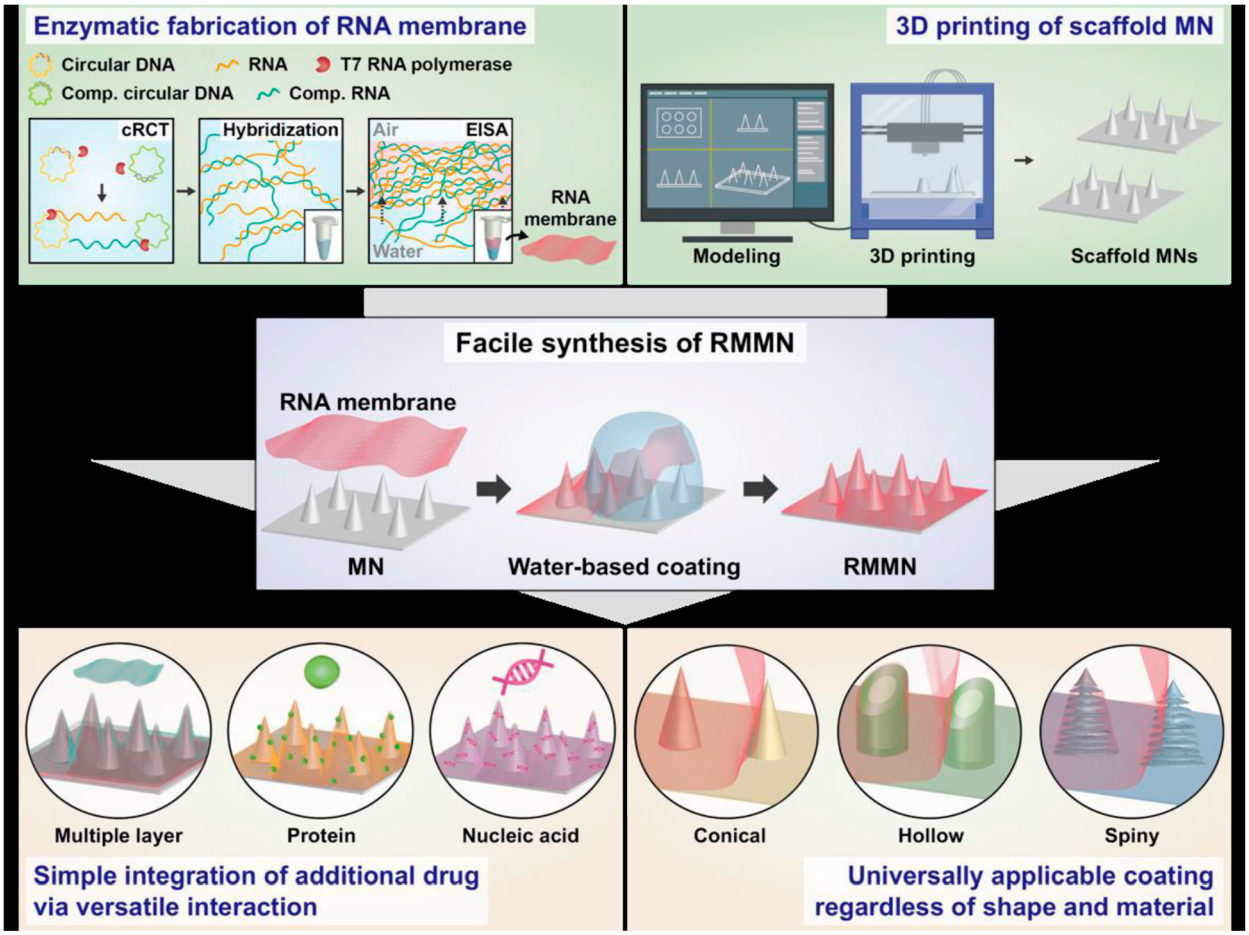

Figure 3. Scheme for the fabrication of versatile RNA-based membrane microneedles (RMNNs). Water-based coating, followed by enzymatically synthesized RNA membrane adsorption, occurs on the 3D-printed microneedles. Custom-made RNA membranes were synthesized by the integration of functional biomolecules and 3D printer-based customization of RMMNs. Reproduced with permission from Kim et al.[70] Copyright 2020, Royal Society of Chemistry.

akin to ink cartridges in an inkjet printer to create the resultant scaffold structure. Printing cell-laden gels, frequently in conjunction with other polymeric materials, is a major characteristic of bioplotter systems, which results in viable and useful scaffolds. The printer extrudes the material from the bioink cartridges using a pneumatic pressurization system. The drawback of this system is the shear stress generated by the nozzles with variable sizes, which might have a deleterious effect on cell viability throughout the printing process.[35] The primary process parameters of a 3D bioplotter are platform temperature, head, cartridge size, build volume, extrusion speed, and pressure.[60]

However, note that through the extrusion of cell-loaded bioinks bioprinting is a cutting-edge method capable of improving the present approaches to tissue bioregeneration in the medical field. As tissue bioregeneration may be created from the patient's own cells, its key benefit is customization to lessen the patient's postoperative difficulties. The printing parameters and, more importantly, the materials affect the effectiveness of bioprinting. Thus, numerous settings can be defined to ensure the best printing stability in terms of the Bioplotter's quality.

2.3. Biomedical Applications of 3D-Printed Materials.

2.3.1. 3D-Printed Materials for Drug Delivery. 3D printing techniques can be used to fabricate personalized oral medicines. This approach involves the fabrication of diverse drug excipients according to patient requirements. Drugs can be tailored to the patient's needs by changing their dosage, morphology, and release behavior. 3D printing of oral medicines involves the following steps. The first step is designing the dosage form by using software. The second step involves mixing the polymer and drug in the desired ratios and loading the blend into a 3D printer. Finally, the dosage form is fabricated in a layerwise manner following the design.

Shi et al. developed oral tablets consisting of a cancer-treating drug, 5-fluorouracil, using a drop-on-powder 3D printing technique.[65] The ink they utilized consisted of 2-pyrrolidone, and the matrix was composed of carbohydrates, vinyl polymers, and $CaSO_4$ hydrates. The tablets were coated with various polymer solutions. Fluorescence microscopy confirmed the even distribution of 5-fluorouracil all over the 3D tablets. Dissolution tests conducted *in vitro* further confirmed that the morphology, composition, and coating material of the tablet affected the release behavior. Thus, this technique can be used to fabricate personalized medicines.

The 3D printing technique has also been used for the delivery of antidiabetic drugs. Gioumouxouzis et al.[66] fabricated a double-layered dosage form comprising two antidiabetic drugs using FDM 3D printing. Metformin was loaded into the Eudragit RL layer, whereas glimepiride was

https://doi.org/10.1021/acsomega.3c03920
ACS Omega 2023, 8, 28002−28025

loaded into the poly(vinyl alcohol) (PVA) layer. X-ray diffraction (XRD) analysis confirmed the encapsulation of drugs into the polymer matrix. By contrast, the dissolution study revealed that adequate amounts of both drugs were released within a desirable period. Thus, this experiment further confirmed the efficacy of 3D printing in the design of personalized dosage forms. 3D-printed oral formulations have been developed for ulcer treatment. Jiang et al.[67] synthesized capsaicin candies via the SLA 3D printing technique. The molds were loaded with materials made of xylitol and detached to obtain solid candies. Poloxamer 188 further augmented the sustained release of capsaicin from the fabricated candies. The efficacy of the candies was tested in rats with oral ulcers, and a healing rate of 97.8% was observed after 7 days' intake of capsaicin candies. Its presence promoted re-epithelization of ulcer tissues and prevented inflammation by reducing inflammatory biomarkers, such as TNF-α and IL-6.

Similarly, Matijašić et al.[68] prepared PVA concentrically compartmental Can-capsules and modular Super-H capsules using FDM. The 3D-printed capsules were packed with powdered ascorbic acid and dronedarone hydrochloride, and their dissolution rates were determined. In an acidic medium, the lag time of the Super-H capsules was found to depend on the thickness of the membrane. The internal layer of the Can-capsules has the potential to resist acid for 2 h, thus rendering it suitable for drug delivery to the small intestine. Thus, these capsules can be used for sustained drug delivery.

3D-printed materials have also been used for the transdermal delivery of drugs and RNA. Khosraviboroujeni et al.[69] synthesized polymeric microneedle arrays made of PLA via FDM 3D printing and injection volume filling. A microneedle was chemically etched to reduce the tip radius to 173 μm. Estradiol valerate was administered. 29.79 $\pm$ 0.03 mg of estradiol valerate was loaded into the 3D-printed microneedle arrays, showing a sustained release for about 7 days. Mechanical tests showed that the force required to fracture the microneedles was greater than that required for penetrating the stratum corneum of the skin. The penetration test confirmed the ability of the microneedle arrays to penetrate the skin without puncturing blood vessels or injecting dermal nerves. Therefore, these techniques can be successfully used for transdermal drug delivery. Kim et al.[70] fabricated a ribonucleic acid (RNA)-based microneedle using 3D printing. Initially, several RNA strands were self-assembled by evaporation to obtain RNA membranes. Next, the membrane was placed on the microneedles irrespective of the morphology and constitution of the scaffold. This is an easy technique for synthesizing microneedles with high concentrations of RNA. The presence of nucleic acids and the porosity of the RNA membranes promoted the loading of similar proteins and nucleic-acid-containing drugs. Sustained dissolution of RNA was achieved using the microneedles. Figure 3 shows a schematic of the fabrication of the versatile RNA-based membrane microneedle.

According to the available literature, 3D printing is an important tool that can be broadly adopted for the engineering of advanced medical devices aimed at controlled drug delivery applications because it provides an avenue for controlling the structural and functional characteristics of the material, which ultimately determines the drug-release performance of these systems. However, 3D-printed controlled drug delivery systems are conceptually new, and further research, along with clinical trials, is required for the adoption of these materials in real-life applications.

2.3.2. 3D-Printed Materials for Tissue Engineering. Several researchers have used various 3D-printed materials for tissue-engineering applications. Cox et al.[71] 3D-printed bone tissue scaffolds from hydroxyapatite and PVA. The nature of the precursor and its effect on the mechanical strength and porosity of the scaffolds were studied. The compressive strength measured for the 3D-printed 55% porous green scaffolds was 0.88 $\pm$ 0.02 MPa. Pores in a material can be modulated to form an interconnected network. In addition, porosity and roughness were introduced into the scaffold because of the packing of the powder particles. These properties promoted osteoconduction and integration *in vivo*.

Similarly, Kabirian et al.[72] fabricated vascular scaffolds from PLA using an FDM 3D printer. The pore size of the meshes could be changed by changing the flow rate of the polymer. Decreasing the flow rate resulted in higher porosity and pore dimensions. The printed scaffolds exhibited uniform structures. Degradation studies confirmed the biocompatibility and mechanical strength of PLA. Thus, the scaffolds can be used as vascular grafts.

Huang et al. fabricated 3D scaffolds exhibiting constant biochemical gradients along longitudinal microchannels using a combined approach of 3D printing and directional freezing.[73] The longitudinal orientation of the microchannels was confirmed by a scanning electron microscopy (SEM) study. Fluorescence studies, in addition to enzyme-linked immunoassay (ELISA) tests, revealed the formation of a constant biochemical gradient. Upon seeding the dorsal root ganglia on the longitudinal segments of the developed scaffold, 81.3 $\pm$ 4.5% neurites were arranged in $\pm$10°. Additionally, the average length of the neurites was 1.5 times on the side of high-nerve growth factor concentration compared to that of low-nerve growth factor. The scaffolds were further used to repair a 15 mm sciatic nerve deficiency in rats. Conclusions drawn from further studies, including transmission electron microscopy (TEM), immunofluorescence staining, and fluoro-gold retrograde tracing, confirmed that the scaffolds can help in regenerating nerves and myelinating regenerated axons. In addition, the results of the von Frey test and sciatic functional index indicated that the scaffold enhanced motor function and sensory recovery. Thus, the developed scaffold can be used to treat nerve injuries.

Using bioplotter printing technology, You et al.[74] fabricated cell-incorporated hydrogels with desirable properties aiming at cartilage tissue engineering. The scaffolds were synthesized using this technique assisted by submerged cross-linking, which facilitated concurrent cell incorporation and pore production within the hydrogels. As it is a one-step process, it is both time-saving and effective for preparing and preserving porous structures. Therefore, a natural biopolymer, sodium alginate, was used to fabricate hydrogels because it can undergo ionic cross-linking in the presence of calcium ions and potentially promote chondrogenic differentiation for cartilage regeneration. The cell-laden sodium alginate solution was dispensed using a 3D bioplotter onto culture plates previously treated with a cross-linker. The *in vitro* results indicated that the cell-impregnated 3D-printed scaffolds led to the survival and growth of chondrogenic cells, thus confirming their usability for cartilage tissue engineering.

Rhee et al.[75] developed 3D-printed tissue implants seeded with primary meniscal fibrochondrocytes using highly dense

https://doi.org/10.1021/acsomega.3c03920
ACS Omega 2023, 8, 28002−28025

Table 3. Biopolymers That Can Be Electrospun Alone without the Use of Any Supporting Polymer

Biopolymer	Molecular weight/brade	Solvent	Electrospinning parameters	ref
Chitosan	106,000 g/mol	Aqueous acetic acid	F.R., 20 μL/min; Voltage, 40 kV	79
	112,000 g/mol	Trifluoroacetic acid	F.R., 0.5 mL h^{-1}; Voltage, 20 kV; Distance, 15 cm	80
Collagen	Type I	1,1,1,3,3,3-Hexafluoro-2-propanol	F.R., 0.02 mL/min; Voltage, 15−20 kV; Distance, 8 cm	81
Gelatin	Bovine skin type B	Acetic acid/double distilled water	F.R., 5 μL/min; Voltage, 15 kV; Distance, 15 cm	82
Xanthan	Cosphaderm X 34	Formic acid	F.R., 0.01 mL min^{-1}; Voltage, 20 kV; Distance, 8 cm	83

collagen hydrogels and studied their morphology, mechanical strength, and cell viability. The mechanical stability of these constructs makes them suitable for supporting and maintaining cell proliferation. Additionally, 3D-printed implants were fabricated with discrete domains and unique mechanical characteristics.

With the adoption of 3D Planning & Printing, researchers can predict severe body part designs and engineering, thereby providing a long-awaited answer(s) to corrective medical science and engineering challenges.

2.3.3. 3D-Printed Materials for Sensing Applications. This section presents a few instances in which 3D-printed materials have been used as sensors. Xiang et al.[76] fabricated graphene nanoplatelet and carbon nanotube-incorporated polyurethane (TPU) composites via 3D printing. The presence of graphene nanoplatelets resulted in the formation of composites with conductive networks. The composites were subsequently used for strain sensing. Owing to the synergy between the carbon nanotubes and graphene nanoplatelets, the printed sensor exhibited higher sensitivity, a more extensive range of detection, and superior stability compared with that of carbon nanotube/TPU or graphene nanoplatelet/TPU composites consisting of 2 wt % of the fillers each. In addition, these sensors can sense strain at various frequencies.

Damiati et al.[77] developed a biosensor that can recognize CD133, a tumor marker found in liver cancer cells. Cancer cell sensing was accomplished by recrystallizing the recombinant S-layer fusion protein on the sensor plane; this helped immobilize the anti-CD133 antibody. The acoustic and hybrid electrochemical biosensors were fabricated by using 3D printing. The hybrid strategy involved a combination of traditional and 3D-printed parts, including a ceramic substrate with noble metals for sensing and 3D-printed capillary channels for guidance.

Using FDM, Cardoso et al.[78] fabricated a biosensor on a graphene-containing PLA surface and used it to detect glucose in the blood via chronoamperometry. The polymer matrix consisting of oxygenated groups offers adequate conditions for enzyme immobilization via glutaraldehyde cross-linking. It exhibited a detection limit of 15 μmol L^{-1}. In addition, when surface treated, the sensor exhibited enhanced electrochemical properties for the detection of uric acid and nitrite. For amperometric detection in the linear range of 0.5−250 μmol L^{-1}, the detection limit was found to be 0.03 and 0.02 μmol L^{-1} for nitrite and uric acid, respectively.

The most widely used 3D printing method for producing biomaterials is FDM, which exactly replicates the designed material along with its predetermined property parameters for precise biomaterial applications. Herein, a thermoplastic filament is used as the feed material for the extruder in a layer-by-layer model.

As discussed above, 3D-printed structures have numerous biomedical applications; however, 3D printing presents several drawbacks that require attention from researchers, as discussed in the following section. We postulate that the integration of 3D printing and electrospinning for the fabrication of advanced biomaterials will solve the problems encountered with the application of 3D-printed biomaterials to a great extent, if not entirely.

2.4. Shortcomings of 3D Printing. Although 3D printing offers several advantages, it also has several shortcomings. The 3D-printed products lack tensile strength based on the printing method. Existing 3D printing techniques fail to fabricate high-resolution filaments, which are important for the production of tissue scaffolds. In addition, as 3D-printed scaffolds have a pore size larger than the cell size, cell seeding and tissue formation are adversely affected. Moreover, only a limited number of appropriate raw materials exist for fabricating products that are biocompatible with human organs. 3D-printed materials have a minimum layer thickness of 16−178 μm, which is unfavorable for the fabrication of biomimetic, functional scaffolds with several hierarchies of designs. In addition, the surface nanotopography cannot be produced by using 3D printing techniques. Thus, the integration of electrospinning with 3D printing may increase the choice of raw materials required for biofabrication, improve the mechanical strength of 3D-printed materials, and favor cell attachment to the scaffolds.

3. CONVENTIONAL ELECTROSPINNING

3.1. Materials for Electrospinning. *3.1.1. Biobased Materials.* Biopolymers are difficult to electrospin, owing to their inherent properties. As they are derived from nature, each batch can vary significantly in terms of crystallinity, electric charge distribution, purity, and molecular weight. Moreover, as these are the major electrospinning parameters, each biopolymer batch must be individually optimized. The choice of the correct solvent was primarily made in the initial stage of electrospinning. Inorganic or organic electrolytes can be used to prevent the formation of hydrogen bonds, which results in highly viscous solutions and unstable jet formation in the presence of an electric field. The chemical modification of biopolymers can generate a repulsive force within the chain, leading to a reduced solution viscosity. In addition, the final electrospun nanofibers may be mechanically weaker and more susceptible to damage. The introduction of natural or synthetic copolymers or chain cross-linking can help overcome these limitations. The most widely used method for electrospinning biopolymers is blending them with other spinnable polymers. This helps to improve the mechanical strength of the final product. Table 3 lists biopolymers that can be electrospun alone without the use of any other polymer.

In another study, Celebioglu and Uyar[84] successfully attempted the electrospinning of cyclodextrin derivatives without using a carrier polymer; these derivatives included methyl-β-cyclodextrin, hydroxypropyl-γ-cyclodextrin, and hydroxypropyl-γ-cyclodextrin. Three solvents were used in the process: dimethylacetamide, dimethylformamide, and water. The experiments indicate that the electrospinning of cyclo-

https://doi.org/10.1021/acsomega.3c03920
ACS Omega 2023, 8, 28002−28025

dextrin is also affected by process parameters similar to those of polymers. Factors such as the solvent type, solution conductivity, and concentration are among the most important process parameters influencing the preparation of nanofibers.

Further, the dynamic light scattering (DLS) measurements revealed that the high viscosity of the solution and the existence of cyclodextrin aggregates promoted the formation of cyclodextrin nanofibers in the absence of carrier polymers. In addition, no fibers could be fabricated from the urea-containing cyclodextrin solution because it significantly destroyed the self-associated cyclodextrin aggregates. The cyclodextrin nanofibers exhibited a higher mechanical strength despite their small, amorphous structure.

The application of electrospun nanofibers as biopolymer nanofibers, along with their other applications, has been demonstrated by researchers in the literature to be a versatile tool for the preparation of biomaterials ranging from drug delivery systems to wound dressing materials, smart implants, and engineering biomaterials for tissue regeneration. However, the integration of electrospinning with 3D printing is projected to be a major approach for solving the challenges of biomedical materials currently faced by researchers and industrialists.

3.1.2. Synthetic Polymers. In addition to natural polymers, several synthetic polymers approved by the Food and Drug Administration can be used for biomedical applications. The hydrophobic nature of synthetic polymers can be balanced by adding hydrophilic polymers, such as PVA, poly(ethylene oxide) (PEO), and polyornithine. The common synthetic polymers used for electrospinning are PLA, PCL, PVA, PEO, and TPU.

The use of synthetically derived biopolymers for electrospun biomaterials for diverse biomedical applications is currently increasing, although TPU is the most widely adopted synthetic biopolymer. Researchers select biopolymers based on their predetermined application niches of interest. Other synthetic biopolymers of recent interest used in this regard are PHBV[85] and PHB,[86] although in most cases they are blends (targeted at property performance enhancement).

3.2. Working Principle. Electrospinning involves the use of an electric force to draw nanofibers from a polymeric solution. Upon application of a high voltage, a liquid drop of the polymer solution leaves the nozzle. Upon applying an extremely high voltage, the droplet becomes charged and distorts from the natural hemispherical shape to a conelike shape called the Taylor cone. Subsequently, a critical point is reached at which the electrostatic repulsion becomes sufficiently strong to overcome the liquid surface tension, thereby resulting in the ejection of a thin liquid jet from the formed cone. Charge repulsion and viscoelasticity regulate the nature of the jets. As the jet diameter is significantly large in the initial stages, viscoelastic forces predominate, thus causing the jet to flow in a straight line. At a critical distance, the charge-repulsive force takes precedence over the viscoelastic force, as the liquid jet extends during conveyance. During this moment, the liquid jet is subjected to extremely forceful bending and whipping movements, which cause the jet width to gradually decrease and the jet solvent to completely evaporate. Finally, the jet is collected on a plate and placed under the syringe. Figure 4 shows a schematic of the electrospinning apparatus.[87]

In the case of coaxial electrospinning, there is an additional set of coaxial nozzles and syringe pumps. However, it follows the same principles.

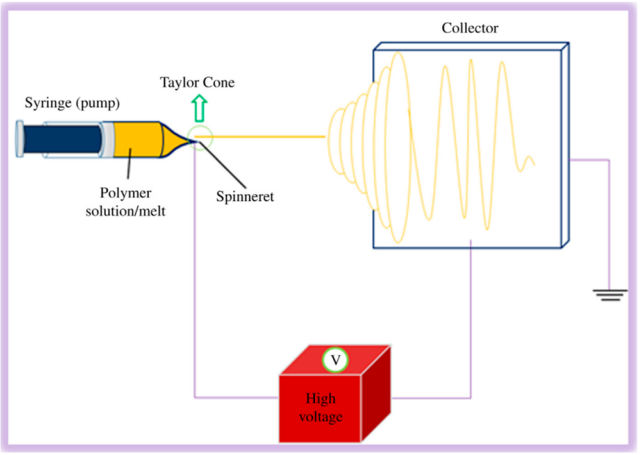

Figure 4. Schematic of an electrospinning apparatus. Reproduced with permission from Orasugh et al.[88] Copyright 2022, Elsevier Science Ltd.

3.3. Electrospinning Parameters. Different electrospinning parameters influence the nature of the nanofibers produced, as presented in Table 4.

Table 4. Electrospinning Variables Affecting the Type of Produced Nanofibers

Parameters	Effect	ref.
Viscosity	Uniform nanofibers are formed by increasing the viscosity of the solution to an optimum level	89
Concentration	The diameter of nanofibers increases with increasing solution concentration	90
Weight of the polymer	More uniform nanofibers are formed by increasing the molecular weight of the polymer	91
Conductivity	As the conductivity decreases, the diameter of the nanofibers formed increases	92
Voltage	Decreasing the voltage results in the formation of fibers with a larger diameter	93
Distance between tip and collector	An optimum distance must be maintained between the tip and collector. Beaded fibers are formed if the distance is too large or too low	94
Flow rate	Increasing the flow rate results in fibers with a larger diameter	95
Type of collector	More aligned fibers can be collected in rotating drums	96
Humidity	Nanofibers with circular pores are formed at high humidity	97
Temperature	Low temperature results in fibers with a larger diameter	96

3.4. Biomedical Applications of Electrospun Nanofibers. *3.4.1. Electrospun Nanofibers for Drug Delivery.* Electrospun nanofibers can be used for sustained transdermal drug delivery. Cui et al.[98] fabricated chitosan (CS) blended PVA nanofibers to deliver drugs through the transdermal route. The electrospun nanofibers were then cross-linked using glutaraldehyde. Experimentally, the cross-linking of the nanofibers resulted in sustained drug delivery without destroying their basic morphology. Cross-linking further enhanced the tensile strength, thermal behavior, and hydrophobicity of the nanofibers. An *in vitro* drug-release study confirmed that the model drug "ampicillin sodium" was released through the Fickian diffusion mechanism. The results exhibited that the electrospun PVA/CS nanofibers can be used for transdermal drug delivery.

https://doi.org/10.1021/acsomega.3c03920
ACS Omega 2023, 8, 28002−28025

Hong et al.[99] reported electrospun cationic ethosome (CE)-loaded silk fibroin nanofibers. Laser scanning confocal microscopy and Fourier transform infrared (FTIR) spectroscopy confirmed the presence of CE within the nanofibers. SEM images showed that CE loading into the fibers did not affect the core morphology. Doxorubicin hydrochloride was used as the model medication, and an *in vitro* drug-release test was conducted in a Franz diffusion cell with mouse skin as the membrane. The results revealed that CE-incorporated nanofibers could deliver drugs at a rate of permeation higher than that of neat silk fibroin nanofibers.

Sun et al. fabricated and applied electrospun epirubicin-incorporated polyacrylonitrile (PAN) nanofibers via a low-energy water-in-oil emulsion electrospinning technique for transdermal drug delivery systems.[100] PAN dissolved in *N*,*N*-dimethylformamide acted as the oil phase, whereas the drug solution acted as the aqueous phase. Tween 80 was used as a surfactant in this process. The drug-release behavior of the nanofibers agreed with the Korsmeyer−Peppas equation. Additionally, an *in vitro* drug-release study confirmed that the fabricated nanofibers exhibit sustained drug-release behavior with 61% cumulative drug release within 24 h. These highly flexible nanofibers also possessed 7.93 MPa tensile strength and, thus, can be used efficiently for transdermal drug delivery.

In addition, electrospun nanofibers can be used for the transmucosal delivery of drugs. Qin et al.[101] developed oral films comprising chitosan and pullulan nanofibers synthesized via electrospinning. Upon increasing the amount of chitosan in the solution, the resultant conductivity and viscosity of the solution increased, thus leading to an initial decrease and a subsequent decrease in the fabricated nanofibers. The FTIR spectrum of the dope showed hydrogen bonding between chitosan and pullulan. XRD analysis indicated that the crystallinity of the starting materials was diminished by electrospinning. Thermal analysis of the samples proved that increasing the chitosan concentration increased the glass transition and degradation temperatures along with their melting points. Further water solubility tests confirmed that the oral films completely dissolved in water within 60 s. To improve the functionality of the films, aspirin was loaded onto the films for oral drug delivery.

Nazari et al. fabricated buccal films with a matrix of hydroxyethylcellulose and Ethocel via electrospinning.[102] Tween 80 was used as a surfactant, and indomethacin was encapsulated within the nanofibers as a model drug. The films were physicochemically tested by using spectroscopic, microscopic, and calorimetric techniques. An *in vitro* drug-release study was performed in a buffer at pH 6.8. As expected, the SEM images showed that the formulation significantly influenced the morphology and diameter of the nanofibers. DSC and XRD analyses confirmed that the drug was loaded into an amorphous state during electrospinning.

By contrast, the FTIR and Raman spectra confirmed the presence of excipients within the fiber matrix. Both the encapsulation and delivery of the drug depended on the composition of the prepared formulation, thus indicating that the dosage can be easily optimized. Thus, electrospinning can be used to fabricate drug delivery systems in which the dosage can be optimized as required.

To deliver antibiotics locally, Teno et al.[103] used electrospun mucoadhesive nanofibrous systems consisting of a multilayered and ciprofloxacin hydrochloride-encapsulated nanofibrous patch to treat bacteria-induced diseases within the oral cavity. The drug-release mechanism of the drug-loaded nanofibers could be altered by varying the ratio of the polyester mixture. The reservoir layer of the patch was studied by using FTIR spectroscopy, SEM, and DSC analyses, which confirmed the uniform distribution of amorphous drugs within the fibrous matrix. To increase the mucoadhesiveness of the fabricated film, the reservoir layer was assembled into a backing layer and an adhesive layer was formed. Examination of this patch based on its drug-release mechanism, adhesiveness, and antimicrobial properties revealed that it possessed good antimicrobial and adhesive properties. Thus, this study demonstrated the use of multilayered nanofibrous patches for the treatment of oral infections.

Drug-loaded electrospun nanofibrous systems are important advanced nanoengineered material systems. Depending on their quality, medications, such as proteins, peptides, antibodies, and small-molecule pharmaceuticals, can be placed inside or on the surface of the nanofibers. Before electrospinning, the hydrophobic medications are mixed with a polymer in an organic solvent. However, the bioactive compounds must be physically absorbed or chemically conjugated onto the nanofiber surfaces. In particular, proteins chemically immobilized on nanofiber meshes promote cell proliferation and differentiation.

3.4.2. Electrospun Nanofibers for Tissue Engineering. In addition to drug delivery, electrospun nanofibers have been widely used for tissue engineering. Sadeghianmaryan et al.[104] fabricated electrospun scaffolds composed of graphene oxide (GO) PU/PCL nanofibers. Initially, PU nanofibers with varying concentrations of PCL and nano-GO were electrospun. Subsequently, multiple techniques were used to characterize the fabricated nanofibers. SEM micrographs revealed that the scaffolds were porous, and the fiber diameter increased with increasing GO loading. The FTIR spectra indicated the presence of both polymers and GO in the scaffold. The scaffolds were biocompatible, and the presence of GO increased the biocompatibility and hydrophilicity of the composite fibers. Thus, these scaffolds are suitable for skin tissue engineering.

In another report, Rad et al.[105] engineered the *Calendula officinalis* extract-loaded PCL/zein/gum arabic nanofibrous scaffold. Three electrospinning methods were used: multilayer, two-nozzle, and suspension. Suspension electrospinning involves the direct addition of the extract to the PCL/zein/GA solution. Two-nozzle electrospinning involves the preparation of PCL/*C. officinalis* and the PCL/Zein/GA layers by using two syringes. Finally, multilayered electrospinning is performed by constructing layer-on-layer structures of PCL/Zein/GA and PCL/*C.officinalis* nanofibers. Beadless nanofibers were electrospun, as confirmed by the SEM images. Moreover, the scaffolds were hydrophilic and possessed the mechanical strength and degradability required for tissue engineering. However, the scaffolds fabricated by multilayer electrospinning possessed a higher tensile strength than those fabricated via suspension electrospinning. In addition, they exhibited slow and sustained release of *C.officinalis*. The incorporation of *C.officinalis* led to the formation of scaffolds with better adhesion, proliferation, antibacterial activity, and biocompatibility than other scaffolds. Therefore, these compounds are suitable for use in skin tissue engineering.

In addition to skin tissue engineering, electrospun nanofibers can be used for nerve tissue engineering. Saudi et al.[106] have

https://doi.org/10.1021/acsomega.3c03920
ACS Omega 2023, 8, 28002−28025

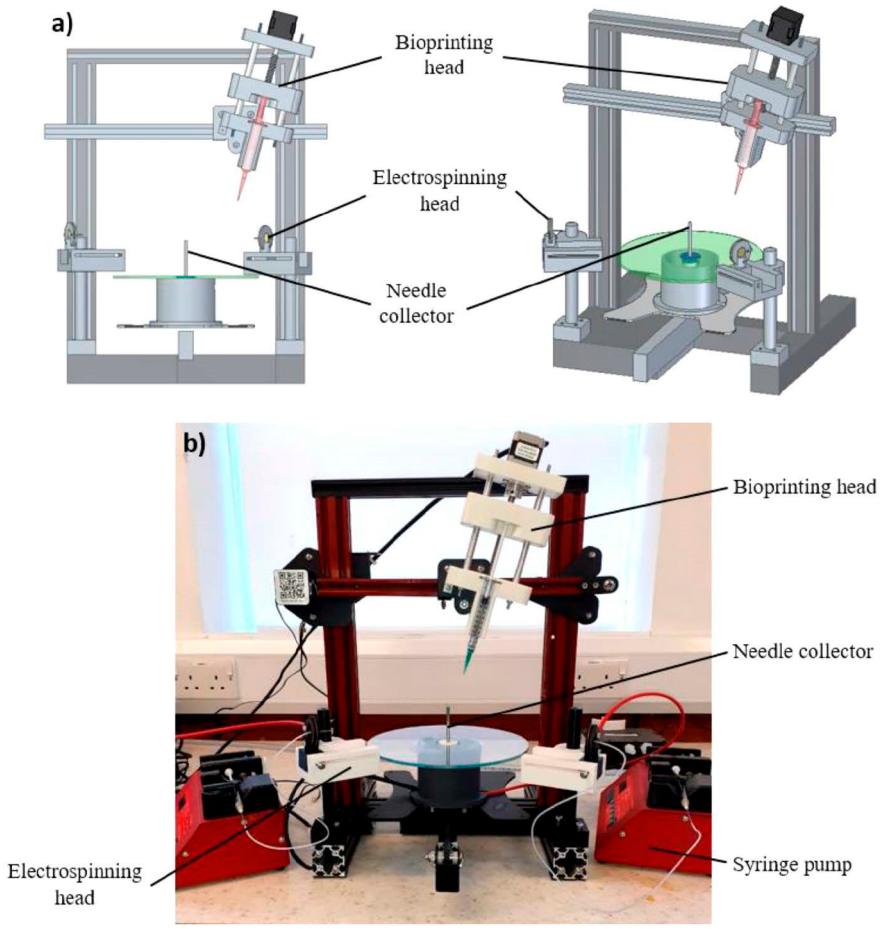

Figure 5. (a) CAD model and (b) original setup of hybrid 3D printing/electrospinning. Reproduced with permission from Fazal et al.[118] Copyright 2021, Elsevier Science Ltd.

also presented the preparation of poly(glycerol sebacate) (PGS) scaffolds for nerve tissue engineering. PVA was used as the carrier polymer for electrospinning PGS nanofibers. Both polymers were mixed in varying ratios for electrospinning, and the nanofibers were thermally cross-linked. The effect of cross-linking on fiber morphology was studied by conducting various physicochemical experiments. Synthesis of PGS at a temperature of 170 °C for a period of 3 h was found to be the ultimate optimized condition for its fabrication. The cells exhibited good proliferation and adhesion. In addition, Young's modulus of the synthesized nanofibers was ideal for nerve tissue engineering.

The use of electrospun nanofibers as a platform for tissue regeneration has proven to be an efficient and effective approach to mimic the ECM, thereby enhancing the attachment and proliferation of cultured cells to these material systems in tissue engineering applications.

3.4.3. Electrospun Nanofibers for Sensing Applications. Electrospun nanofibers are often used in biosensors. In this regard, Paimard et al.[107] developed a label-free electrochemical immunosensor that can be used to detect a significant tumor biomarker, the carcinoma-embryonic antigen. Coaxial nanofibers were electrospun on the electrode surface and further incorporated with multiwalled carbon nanotubes and gold nanoparticles. Subsequently, the carcinoma embryonic antigen was immobilized. The nanoparticle-decorated honey nanofiber exhibited high sensitivity toward the tumor biomarker in the concentration range of 0.4−125 ng mL^{-1} and detection limit of 0.09 ng mL^{-1}. Thus, the immunosensor could detect trivial changes in biomarker concentrations.

Similarly, Tripathy et al.[108] developed an electrochemical biosensor that can detect single-point DNA mutations that cause several genetic disorders, including cancer. Graphene-loaded manganese oxide nanofibers (GMnO) were used for sensing. The nanofibers were highly sensitive to any confined change in conductivity owing to their charge-transfer resistance. The low bandgap of manganese oxide and high charge transfer kinetics of graphene are responsible for the sensitivity of the sensor. To verify this, the BRCA1 gene-specific point mutation was detected. The detection limit for the DNA, as mentioned earlier, was found to be 0.8 ± 0.069 pM. In conclusion, by simply choosing an appropriate functionalization protocol, any mutation in DNA can be detected using the sensor.

Ismail et al.[109] fabricated an electrochemical sensor with an electrode made of screen-printed carbon modified with electrosprayed gold nanoparticles and PAA/PAN electrospun nanofibers to monitor glucose. The incorporation of AuNPs into the nanofibers increased their conductivity. The sensor exhibited a detection limit of 0.756 mM and sensitivity of 1.043 $\mu A\ cm^{-2}\ mM^{-1}$ in the concentration range of 2−16 mM. This report, being one of the earliest works that modified an SPCE for glucose sensing, had a performance that was on par with other electrode types, such as glass carbon electrode

https://doi.org/10.1021/acsomega.3c03920
ACS Omega 2023, 8, 28002−28025

Table 5. Ways to Fabricate 3D-Printed/Electrospun Composites[a]

Method of combination	Advantage(s)	Disadvantage(s)
Electrospinning onto 3D-printed scaffolds	Ease of manufacturing and uncomplicated processing;	Maldistribution of electrospun fibers on complicated scaffolds;
	Scaffolds with complex 3D geometries and personalized structure; Scaffolds with enhanced mechanical performances	Difficult to form strong adhesion between electrospun fibers and 3D-printed scaffolds
3D printing onto electrospun fibers	Ease of manufacturing and uncomplicated processing; Efficient preparation of tubular scaffolds; Scaffolds with enhanced mechanical properties	Only suitable for fabricating planar- and tubular-shaped products
Alternate use of 3D printing and electrospinning	Scaffolds with ECM-like internal structure; Cell deposition in accurate locations in scaffolds; Multimaterials and multiscale manufacturing; Scaffolds with enhanced mechanical properties	Complexity to produce scaffolds with various shapes
Electrospun fibers as inks of 3D printing	Scaffolds with personalized shapes;	Uncontrollable arrangement of electrospun fibers;
	Scaffolds with enhanced mechanical properties; Uniform distribution of nanofiber segments in 3D-printed scaffolds; Good bonding between electrospun fibers and 3D-printed scaffolds	Nozzle blockage
Decorating/infusing 3D-printed scaffolds with electrospun nanofiber segments	Uniform distribution of nanofiber segments on 3D-printed scaffolds	Uncontrollable arrangement of electrospun fibers
Fabrication of electrospun scaffolds on/in 3D-printed collectors/templates	Fast and precise production of electrospun fiber scaffolds and electrospun membranes with controllable geometric shapes and patterned structures	Insufficient mechanical properties for specific applications
Combined use of different components prepared by electrospinning and 3D printing, respectively	Scaffolds with complex 3D geometries and personalized structure; Scaffolds with enhanced functionality and extensive applications	–
Platforms combining 3D printing and electrospinning techniques	High degree of integration; High level of automation; Complex forming technology	–

[a]Partially reproduced with permission from ref 119. Copyright Wiley, 2022.

(GCE) and ITO glass. A reliable nonenzymatic glucose sensor can also be created using this modification of the screen-printed electrode.

Based on the above discussion, we can conclude that electrospun nanofibers have a plethora of biomedical applications. However, this technique has a few drawbacks, which are discussed in the following section. We hypothesized that the issues associated with the use of 3D-printed biomaterials can be significantly reduced if not completely eliminated by combining electrospinning and 3D printing for the creation of advanced biomaterials.

3.5. Shortcomings of Electrospinning. Electrospinning is widely used in biomedical applications but has several drawbacks. These include meager cell infiltration and migration, owing to the dense packing of scaffold fibers. In addition, the mechanical strength of the nanofibrous scaffolds is low. Electrospinning renders the fabrication of devices with a variable shapes challenging. Conventional electrospinning lacks the potential to produce predetermined 3D structures. Thus, integration with 3D printing aids in the construction of 3D structures with higher mechanical strengths.

4. COMBINATIONAL APPROACH: 3D PRINTING AND ELECTROSPINNING

4.1. Techniques to Fabricate 3D Printed-Materials/Nanofibers Composite Scaffolds. A combination of 3D printing and electrospinning techniques is the most favorable option available to overcome the drawbacks of each technique and fabricate products with enhanced biomedical applications. There are different ways to combine the approaches of electrospinning and 3D printing to develop products for biomedical applications. One of the most straightforward techniques is fabricating 3D-printed structures and electrospun nanofibers directly on its surface.[110−112] The second method involves 3D printing on tubular or flat nanofibers.[113,114] Another approach is to develop hybrid scaffolds by alternatively using 3D printing and electrospinning.[115] Here, a layer is initially fabricated by the 3D printing process, and electrospun nanofibers are deposited over it. Subsequently, 3D printing and electrospinning were performed alternatively to combine the layers. In addition, nanofiber sheets can be initially synthesized and inserted between stacks of 3D-printed structures.[116] In addition to these techniques, another combinational approach involves the use of electrospun nanofibers as ink for the 3D printing process.[117] This leads to the formation of scaffolds with adequate mechanical strength, size, and microstructure.

To integrate 3D printing and electrospinning platforms, a hybrid setup was reported by Fazal et al.,[118] as shown in Figure 5. A modified version of the Creality3D Ender 3D printer was used to produce small-diameter vascular grafts. It consists of two electrospinning heads and one bioprinting head and can fabricate layered electrospun fibers and a cell-laden hydrogel.[118]

Table 5 presents all combinational approaches along with their merits and demerits.[119]

4.2. 3D-Printed Materials/Nanofiber Composites and Their Biomedical Applications. *4.2.1. 3D-Printed Materials/Nanofibers Composites for Tissue Engineering.* As previously stated, 3D printing technology can be used to synthesize scaffolds for tissue regeneration. However, as the maximum print resolution achieved for this technique is approximately 300 μM, the meshes of 3D-printed scaffolds are large for the adherence of most cells. By contrast, although

https://doi.org/10.1021/acsomega.3c03920
ACS Omega 2023, 8, 28002−28025

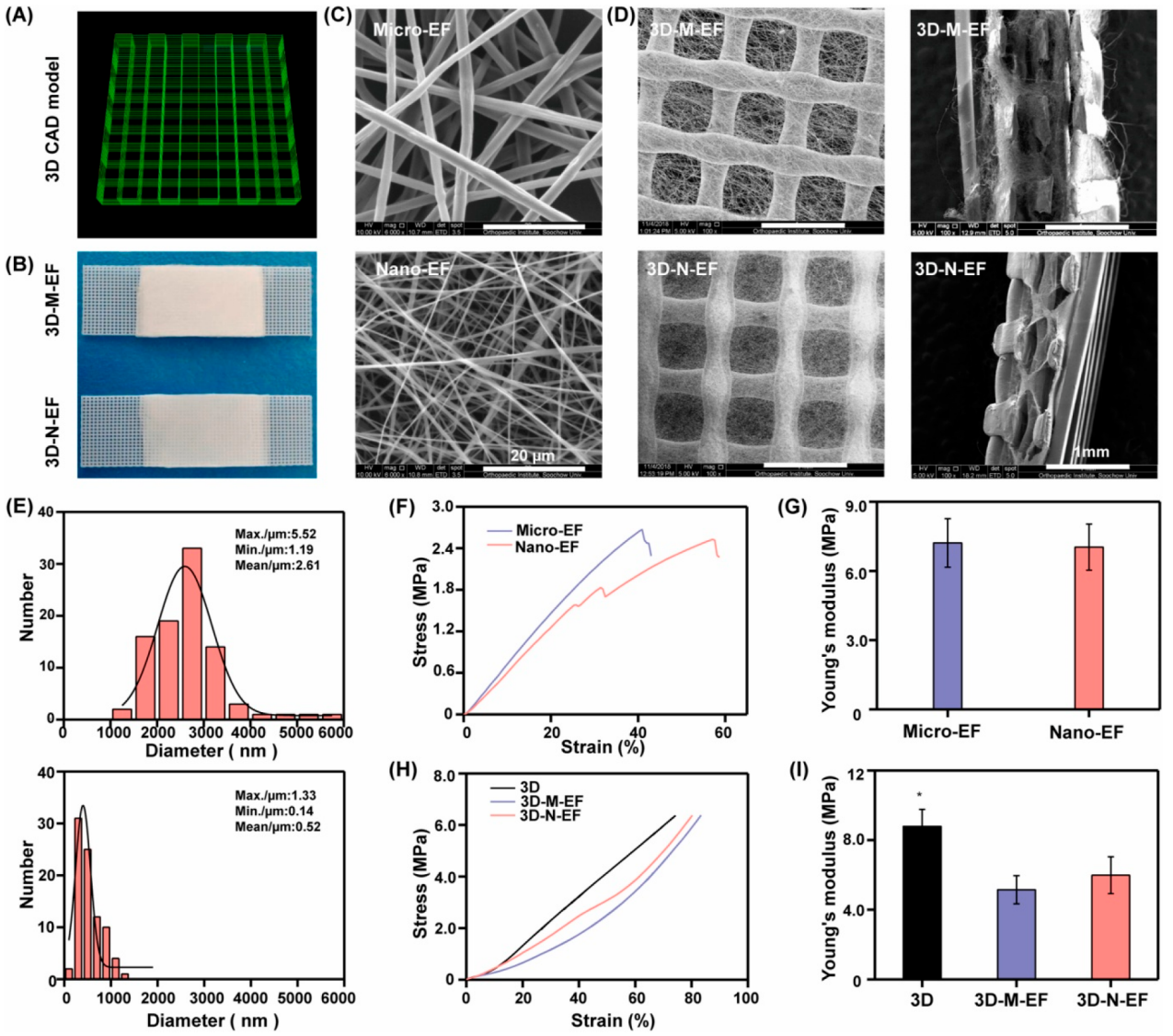

Figure 6. (A) 3D computer-aided design for scaffold fabrication. (B) Images of the 3D-M-EF and 3D-N-EF scaffolds. (C) SEM images of the M-EF and N-EF scaffolds. (D) SEM images of the 3D-M-EF and 3D-N-EF scaffolds. (E) Diameter histogram of the M-EF and N-EF scaffolds. (F), (G) Young's modulus and stress−strain curves of the M-EF and N-EF scaffolds, respectively. (H),(I) Young's modulus and stress−strain curves of the 3D, 3D-M-EF, and 3D-N-EF scaffolds, respectively. *$p < 0.05$: in comparison to 3D-M-EF scaffolds and 3D-N-EF scaffolds ($n = 3$). Reproduced with permission from Liu et al.[124] Copyright 2021, Elsevier Science Ltd.

electrospun scaffolds have a high porosity, their pore dimensions are sufficiently small for cell migration and infiltration. Consequently, numerous researchers are investigating various ways to increase the pore size for cell infiltration. Herein, we discuss the role of 3D-printed materials/nanofibers composites. The combination of electrospinning and 3D printing has been extensively used in tissue engineering.

4.2.1.1. 3D-Printed Materials/Nanofibers Composites for Bone Repair. The restoration of bone tissue is a major clinical issue that has a high morbidity rate in trauma patients and imposes a significant economic burden. Yu et al.[116] presented the 3D printing of PCL scaffolds and infused meshes with a dispersion of PCL/gelatin nanofibers. SEM was used to characterize the surface morphologies of the scaffolds. Evidently, it possessed a high porosity of 79.32 ± 8.32% and a compressive modulus of 30.50 ± 0.82 MPa. The composite scaffolds exhibited good biocompatibility and enhanced cell proliferation. In conclusion, this scaffold can be used to repair bone tissues. Zhu et al.[120] fabricated an intervertebral disc (IVD) scaffold using 3D printing and electrospinning. The IVD frame was 3D-printed using PLA. The annulus fibrosus structure was replicated using poly(L-lactide)/octa-armed polyhedral oligomeric silsesquioxane fibers. Finally, the morphology of the nucleus pulposus was simulated using bone marrow mesenchymal stem cells containing gellan gum/poly(ethylene glycol) diacrylate hydrogels. The porosity, mechanical strength, and compression modulus of the IVD scaffold matched those of natural IVD and could be modulated through 3D printing. The annulus fibrosus consisted of concentrically arranged fibers that could endure the tension caused by the distortion of the nucleus pulposus. In addition, an even distribution of bone marrow mesenchymal stem cells was observed in the hydrogel, thus providing good cell viability. Further testing in animal models confirmed that the IVD scaffold could regulate the disc space and generate ECM.

https://doi.org/10.1021/acsomega.3c03920
ACS Omega 2023, 8, 28002−28025

Liu[121] synthesized a double-layered scaffold consisting of an electrospun PCL/gelatin nanofibrous layer combined with PCL/gelatin/nanohydroxyapatite (nHA) scaffolds. On conjugating heparin with the PCL/gelatin membrane, good adhesion and growth of L929 fibroblasts occurred. The PCL/gelatin/nanohydroxyapatite scaffold facilitated the adhesion, growth, and osteogenic differentiation of bone marrow mesenchymal stem cells. After 20 weeks of treatment, the double-layered scaffolds promoted bone regeneration.

Naghieh et al. utilized the FDM technology to develop PLA microstruts and electrospun gelatin-forsterite nanofibers.[122] The elastic modulus of the prepared scaffold was much higher than that of the pristine scaffold. The generation of calcium-phosphate-like residues on the scaffold surface confirmed the influence of the nanofibrous membrane on the enhanced bioactivity of the scaffolds. Considering the biological and mechanical characteristics of the scaffold, it is a promising material for bone-tissue regeneration. Similarly, the advantages of two widely used biomaterials, PLLA and gelatin, and two different scaffold fabrication methods, 3D printing with FDM and electrospinning, were combined by Rajzer et al.[110] to produce a novel multifunctional layered scaffold for the reconstruction of subchondral bone and nasal cartilage. The otolaryngologists' issue with securing the nasal cartilage implant using a needle and thread was addressed by the pore diameter of the scaffolds created by 3D printing technology. Gelatin nanofibers formed the top layer, and porous PLLA produced by 3D printing formed the bottom layer of the hybrid scaffold. The mineralization capacity of the scaffold was assessed in an artificial bodily fluid.

Using an FDM 3D printer, Saniei et al.[112] fabricated PLA screw implants and modified their surfaces to improve cell affinity and bioactivity. The screws were coated with electrospun PVA-nHA nanofibers with varying amounts of nHA. The diameters of the electrospun nanofibers ranged between 263.1 and −326.3 nm. The bioactivity of the scaffolds was tested using a cytotoxicity assay and screw immersion in simulated body fluid. The nanofibers enhanced the attachment and growth of MC3T3-E1 cells. Huang et al.[123] integrated a screw-assisted 3D printing technique with rotational electrospinning to fabricate microporous PCL structures with largely aligned electrospun nanofibers. The 3D-printed structures possessed uniform geometry, and the alignment of the nanofibers was enhanced with an increase in the electrospinning rotational velocity. The presence of the electrospun nanofibers did not significantly influence the mechanical strength of the hybrid scaffolds. As confirmed by *in vitro* test results, higher seeding and growth of human adipose-derived stem cells were facilitated by high-density electrospun nanofibers. In addition, the presence of nanofibers increases the stretchability and elongation of the cell morphology. It exhibited better expression of the osteogenic markers.

By contrast, 3D-printed PCL/PLLA nanofibrous (3D-N-EF) and microfibrous (3D-M-EF) composites and their osteogenic and immunomodulatory effects were examined by Liu et al.[124] Evidently, 3D-M-EF scaffolds exhibited more polarization of RAW264.7 cells toward alternatively activated macrophages (M2) via PI3K/AKT signaling. This increases the expression of BMP-2 and VEGF. Also, the 3D-M-EF scaffolds supported osteogenesis, angiogenesis, and hastened regeneration of bones, and the results are summarized in Figure 6.

The available literature reports the excellent architecture and proficient property performance of scaffold materials engineered by the amalgamation of 3D printing and electrospinning. Materials prepared in this regard not only are robust but also provide the desired platform to mimic the actual bone structure for facile regeneration of bone tissues.

4.2.1.2. 3D-Printed Materials/Nanofibers Composites for Muscle Tissue Repair. Skeletal muscle comprises a uniaxial arrangement of myotubes and an extensive distribution of blood capillaries. To mimic these properties, Yeo et al.[125] 3D-printed PCL/collagen struts to support human umbilical vein endothelial cell (HUVECs)-loaded alginate electrospun nanofibers. The HUVEC-laden nanofibers exhibited a uniform distribution of cells, HUVEC proliferation, and 90% cell viability. In addition, C2C12 cells were seeded onto the nanofibers and cocultured to promote myoblast regeneration. The presence of both HUVECs and myoblasts improved the expression of myogenesis-specific genes compared with a scaffold consisting of myoblasts.

The combination of 3D printing with electrospinning has thus far been shown to be an effective and efficient tool for the preparation of scaffold mimetics of muscle ECM upon application. However, currently, the literature within this application niche is limited, which calls for more research.

4.2.1.3. 3D-Printed Materials/Nanofibers Composites for Nerve Tissue Repair. Peripheral nerve damage is a common clinical condition that frequently requires surgical nerve restoration. Tissue-engineered conduits thus far are essential for nerve repairs. Despite recent advances, the creation of translational biomimetic neural conduits is extremely difficult. For instance, Liu et al.[126] synthesized a three-layered conduit by combining processes such as electrohydrodynamic (EHD) jet printing, electrospinning, and dip coating. The innermost layer was composed of PCL filaments synthesized using EHD jet printing. The midlayer comprised dip-coated gelatin hydrogels, and the topmost layer consisted of PCL nanofibers. This approach helped fabricate a mechanically tuned trilayered conduit that was highly compatible with vascular cells.

In another study, electrospun poly(lactide-*co*-caprolactone) (PLCL)-based elastic nerve guidance conduits (NGCs) were grafted with 3D-printed collagen hydrogels.[114] The NGCs were tested for axonal regeneration and remyelination in a rat model of sciatic nerve injury. Alignment of the collagen hydrogels guided nerve regeneration, thereby promoting nerve regeneration. Usal et al.[127] 3D-printed a nerve guide made of PCL from an electrospun mat comprising gelatin-poly(3-hydroxybutyrate-*co*-3-hydroxyvalerate) seeded with PC12 and Schwann cells. The physical characterization of the fibers revealed that the fibers had an average diameter of 382 ± 25 μm and a pore size of 675 ± 40 μm. The electrospun nanofibers have an alignment degree of 7°, thus demonstrating their guidance abilities. On the 14th day, the migration of PC12 cells from the nerve guide proximal to the distal end was observed, whereas Schwann cells remained seeded. Approximately 95% of PC12 cells were aligned and survived after 28 days. Histological studies have shown that most new tissues are organized using mats and cell-free guides. Thus, 3D-printed nerve guides have the potential to treat nerve injuries.

To improve the biocompatibility of the fabricated objects, Namhongsa et al.[128] prepared scaffolds made of PLCL and PLGA by integrating 3D printing and electrospinning. The scaffolds were then coated with PPy to improve their biocompatibility. The average pore sizes of the PLCL- and PLGA-based scaffolds were 289 and 287 nm, respectively. Blending the polypyrrole with the polymeric solution enhanced

https://doi.org/10.1021/acsomega.3c03920
ACS Omega 2023, 8, 28002−28025

its hydrophilic, conductive, and noncytotoxic nature compared to the noncoated scaffold. Both scaffolds preserved their conductivity for approximately 9−15 weeks. In addition, the PLGA-based scaffolds exhibited better cytocompatibility than the PLCL-based scaffolds. Furthermore, polypyrrole-based scaffolds exhibited reduced membrane leakage and necrotic tissue.

According to the literature, 3D printing of composite nanofibers has been established as a valuable tool for the engineering of nerve tissues, which currently poses great challenges to the medical field. We believe not only that the integration of electrospinning and 3D printing will solve the problems associated with nerve repair but also that materials fabricated via this approach will serve well in other biomaterial niches.

4.2.1.4. 3D-Printed Materials/Nanofibers Composites for Cartilage Repair. As in the previous case, the limited potential of the cartilage to regenerate itself makes cartilage restoration a perennial concern. Tissue engineering is a novel and efficient method of cartilage repair. Liu et al.[129] fabricated composite scaffolds via electrospinning and 3D printing. Poly(lactic-*co*-glycolic acid) nanofibers were initially synthesized and integrated into hydroxybutyl-chitosan hydrogels. The inclusion of nanofibers into the hydrogel resulted in a short gelation time of 15 s at 37 °C and promoted cell differentiation. Subsequently, a 3D-printed PCL framework consisting of microchannels that provided support and promoted the exchange of substances was fabricated by coprinting PCL with the sacrificial polymer Pluronic F-127. The prepared hydrogel was injected into the PCL framework. This resulted in the fabrication of mechanically robust scaffolds. These scaffolds induced *in vivo* chondrogenesis. It presents an ideal microenvironment suitable for cartilage differentiation and growth, thus proving its application in cartilage tissue engineering. Similarly, Farsi et al.[130] fabricated PLA scaffolds via FDM 3D printing and coated them with PVA/HA nanofibers. The scaffold exhibited hydrophilicity, owing to the presence of PVA and hyaluronic acid. Additionally, the nanofibrous coating increased the elastic modulus and tensile strength of the scaffolds. The results of the MTT assay proved that the scaffolds were nontoxic. The scaffolds further promote the adhesion of chondrites to the scaffolds. Thus, the synthesized scaffolds can be used for cartilage regeneration. Another report presented the fabrication of cartilage decellularized matrix (CDM)-based scaffolds via 3D printing. Gelatin/poly(lactic-*co*-glycolic acid) (PLGA) nanofibers were electrospun and homogenized. The dispersed nanofibers were further blended with a CDM and hyaluronic acid mixture. Scaffolds were 3D-printed from nanofibers incorporated in the CDM-based ink. The loading of nanofibers into the CDM ink imparts toughness and stiffness. In addition, the scaffolds exhibited *in vitro* and *in vivo* biocompatibility and articular cartilage repair.[131]

Yuan et al.[132] prepared 3D-printed tracheal constructs consisting of dispersed poly(L-lactide)/gelatin short nanofibers. A scaffold consisting of 1 wt % of nanofibers exhibited less density, better water absorption capability, apposite rate of degradation, and good mechanical strength resembling that of the native trachea. The scaffolds were biocompatible and promoted *in vitro* proliferation and infiltration of chondrocytes. Mice were subcutaneously implanted in the mouse models for 4−8 weeks. A histological study of the scaffolds explanted after 4 weeks revealed that the constructs maintained their structure and promoted the creation of neovessels. In addition, the cell scaffolds exhibited the gradual formation of cartilage tissues that matured over time. Thus, the scaffolds have both mechanical strength and an ECM-like structure, which is beneficial for tracheal regeneration. Kang et al.[133] constructed a strong antibacterial tracheal graft consisting of 3D-printed TPU skeletons enveloped with electrospun PLA nanofibers. Graphene oxide functionalized with an ionic liquid (GO-*g*-IL) was fabricated and exhibited high mechanical strength and hydrophilicity. When the PLA membranes were surface-modified with GO-*g*-IL, they exhibited better antibacterial properties than those modified with IL or GO. The sharp edges of GO help break down the cytomembrane of bacteria, whereas ionic interactions between cationic groups in the case of IL and negatively charged phosphate groups of the bacterial membrane lead to cell death. Improved cell growth, adhesion, and infiltration were observed upon seeding phenotypically shaped fibrous membranes with L929 fibroblasts. *In vivo* tests using rabbit models revealed that the membranes exhibited good biocompatibility and tissue regeneration.

The current application of 3D-printed material/nanofiber composites for cartilage repair is increasing, primarily owing to the precision of the fabricated materials mimicking the tissues aimed at repair. In addition, more research is necessary in this niche, particularly holistic investigations involving lab-to-industrial-scale preparations for real-life applications.

4.2.1.5. 3D -Printed Materials/Nanofibers Composites for Vascular Graft Applications. With respect to vascular graft materials, Mayoral et al.[134] designed a patient-specific patch using a hybrid 3D print in conjunction with vascular smooth muscle cell (VSMC) differentiation. They assessed the most hemodynamically effective aortic patch surgical repair using computational modeling and medical images of a 2-month-old girl with aortic arch hypoplasia. A hybrid FDM technique along with electrospinning was used to print scaffolds based on the geometry of the 3D patch. Multipotent mesenchymal stem cells (MSCs) were implanted into the scaffold to mature into VSMC. The graft had a porosity gradient ranging between 80 and 10 μm, thus facilitating cells to penetrate the entire thickness of the patch, and it demonstrated acceptable resistance to normal aortic pressure (burst pressure of 101 ± 15 mmHg). The bioscaffolds displayed good cell survival and sufficient functional vasoactive response to endothelin-1 on days 4 and 12.

Another example is the design and engineering of 3D-printed blood vessels comprising chitosan/PCL electrospun nanofibers coated with strands of PCL by Lee et al.[135] Initially, PCL nanofibers were mixed with chitosan, and the resultant composite was coated with PCL strands. A combination of electrospinning and rapid prototyping techniques was used to fabricate a blend of chitosan and PCL. SEM and FTIR spectroscopies were used to characterize the scaffolds. The contact angles and mechanical strengths of the fabricated vessels were investigated. The results demonstrated that printing PCL strands on the nanofibers increased the mechanical strength. Huang et al. explored the synthesis of a three-layered fibrous structure for fabricating vascular grafts.[136] The innermost layer comprised 3D-printed, mostly aligned, robust fibers, whereas electrospun fibers formed the midlayer of the graft. Additionally, the outer layer consisted of coelectrospray mixed fibers. The grafts were implanted *in vivo*. The aligned fibers within the graft enhanced the growth and movement of the endothelial cells. The outermost layer

https://doi.org/10.1021/acsomega.3c03920
ACS Omega 2023, 8, 28002−28025

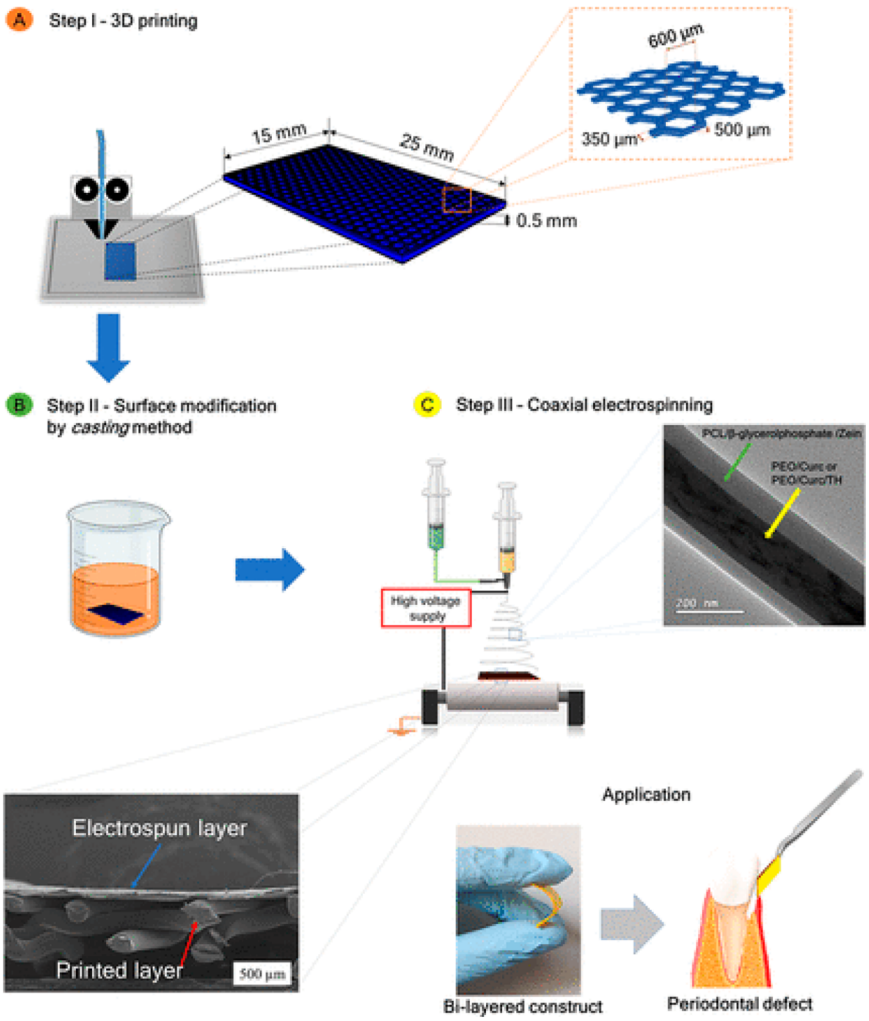

Figure 7. (A) 1st step: 3D printing of PLA honeycomb-like structures. (B) 2nd step: Modifying honeycomb walls with zein film via the casting technique. (C) 3rd step: Electrospinning coaxial nanofibers on one side of 3D-printed modified structures. Reproduced with permission from dos Santos et al.[141] Copyright 2022, ACS Publications.

facilitated the migration of cells into the scaffold following implantation. This graft supported *in vivo* cell proliferation along with infiltration and thus had advantages over conventional electrospun grafts, which exhibit insufficient porosity and poor cell penetration.

The available literature on the adoption of 3D printing and electrospinning as effective approaches for the fabrication of biomaterials aimed at vascular graft materials is currently limited, although this approach has been established as an outstanding system for vascular graft material fabrication.

4.2.1.6. 3D-Printed Materials/Nanofibers Composites for Skin Tissue Repair. The structure and function of the skin must be restored as soon as possible after an injury, as it is the first line of defense against any attack from the outside. 3D-printed materials/nanofibers composites have also aided in skin tissue regeneration. For instance, Chen et al.[137] fabricated PLA/gelatin nanofibrous scaffolds via 3D printing using a hand-held electrospinning apparatus. Various physicochemical tests, such as XRD, FTIR, and SEM analyses, water vapor transmission rate, and water contact angle measurements, were conducted. Cytotoxicity tests were conducted to assess the toxicity and biocompatibility of the scaffolds. The feasibility of the scaffolds was tested in wounded mice as an artificial skin demonstration. Another example was presented by Miguel et al.,[138] who also constructed 3D-printed skin using a combinational approach. A top layer, electrospun from a mixture of PCL and silk sericin, was created to imitate the properties of the epidermis and guard against dehydration and other dangers. The dermis was subsequently created by the layer-by-layer printing of a chitosan/sodium alginate hydrogel. *In vitro* studies confirmed that the composite can be used as a skin substitute.

Although literature on the use of 3D printing and electrospinning as successful methods for the fabrication of biomaterials intended for skin tissue repair is currently scarce or limited, available literature has established this method as an excellent system for the fabrication of materials for skin tissue repair.

4.2.2. 3D-Printed Nanofiber Composites for Sensors and Actuators. The adoption of 3D-printed nanofibers in actuators and sensors has not been excluded from the drive toward the utilization of 3D -fabricated systems in advanced materials science and technology. Lee et al.[139] aimed to fabricate a sensor by integrating 3D-printed elastomeric sheets with electrospun nanofibrous mats. Polydimethylsiloxane (PDMS) molding was used to synthesize the elastomeric sheets. 3D

https://doi.org/10.1021/acsomega.3c03920
ACS Omega 2023, 8, 28002−28025

scanned skin was used as the basis of the 3D-printed mold assembly design, which possessed one upper part and one lower part interconnected by a hinge. Owing to their structure, the skin-conformal PDMS constructs can be molded and demolded repetitively. It was further integrated with an electrospun nanofibrous mat of piezoelectric polymer poly(vinylidene fluoride trifluoroethylene). The sensitivity and linear relationship between the input and output of the 3D-printed composite are identical with those of a flat sensor. It responded to minute physical stimuli, thus, demonstrating its potential as an excellent wearable sensor. In addition, Chen et al.[140] proposed an approach that combined electrospinning and 3D printing to produce shape-morphing hydrogels with rapid deformation and improved the designability of 3D shapes. Intricate patterns were imprinted on the mesostructured electrospun membranes. These patterns control the internal tensions caused by the swelling/shrinkage mismatch in the in-plane and interlayer regions, thus leading to morphing behaviors of the electrospun membranes in response to environmental changes. This method allows the construction of various rapidly deformed hydrogel actuators with distinctive responsive behaviors such as the formation of 3D structures in reversible or irreversible ways, folding of 3D tubes, and fabrication of 3D configurations with multiple low-energy states. Although poly(*N*-isopropylacrylamide) was used as the model in this study, this method can be used with various smart hydrogels, enhancing the design of quickly deformed hydrogel actuators.

The adoption of 3D-printed composite nanofibers in actuator and sensor systems in advanced materials science and technology has been established by researchers as per the literature, though in a few instances, the results have proven that sensors and actuators can indeed be fabricated using 3D printing technology.

4.2.3. 3D-Printed Nanofiber Composites for Drug Delivery. 3D printing technology has been developed to engineer predetermined systems for advanced material applications, such as drug-loaded systems for controlled drug delivery. In this light, Santos et al.[141] used the combinational approach of 3D printing and coaxial electrospinning for tissue regeneration and drug delivery (Figure 7). Initially, a core−shell nanofiber, which consisted of curcumin, the drug tetracycline hydrochloride, and PEO as the core of the nanofiber, was electrospun. The shell of the fiber consisted of zein and β-glycerol phosphate, whereas poly(ε-caprolactone) was the carrier polymer. The coaxial nanofibers were collected over a 3D-printed structure made of poly(lactic acid), zein, and curcumin to yield a dual-layered structure that imitates the periodontal tissue. The physicochemical characteristics and drug-release profiles of the 3D-printed/electrospun composite could be controlled by changing the zein concentration in the nanofiber shell layer, which altered the diameter from 150 to 400 nm. The fabricated dual-layered construct exhibited sustainable delivery of the drug for a period of over 8 days and was found to be biocompatible with human oral keratinocytes. Additionally, the construct had antibacterial properties against bacteria including *Treponema denticola* and *Porphyromonas gingivalis*, which cause periodontitis. Thus, the membrane had the potential for the sustained delivery of two drugs along with periodontal tissue regeneration.

In another instance, drug-releasing cuboid frames via a combinational approach aimed at repairing alveolar bone were reported by Chou et al.[142] The cuboid frames consisted of polylactide cages and drug-loaded nanofibers that imitated the structure of the ECM of bone tissues.[142] The physicochemical properties of the 3D-printed frame and electrospun nanofibers were assessed. High-performance liquid chromatography was used to study the *in vitro* and *in vivo* drug-release behaviors of the nanofibers. The *in vivo* drug-release efficiencies of the frame and nanofibers were studied in a rat model of alveolar bone defects. The prepared frames exhibited sustained delivery of drugs such as amoxicillin and ketorolac for approximately 4 weeks. In addition, animals implanted with a drug-releasing frame showed better movement than those without such implantations. Histological analysis confirmed that these constructs exerted no adverse effects. Therefore, this combined approach can be used in various maxillofacial applications.

Another group of researchers reported the fabrication of biodegradable polylactide cages via 3D printing to facilitate the fixation of bones and antibiotic-incorporated poly(D,L)-lactide-*co*-glycolide nanofibers for healing comminuted metaphyseal fractures in a rabbit femoral model.[143] The drug-release profiles of ceftazidime and vancomycin from the nanofibers were examined, and the mechanical characteristics of the 3D-printed cages were studied. An *in vivo* study was conducted using rabbit models of complex metaphyseal fractures. The results showed appreciable amounts of ceftazidime and vancomycin in the local tissue fluid near the fracture site for approximately 3 weeks. *In vivo* studies demonstrated that the synthesized cage exhibited maximal bending strength, a leg length ratio, and superior cortical integrity. These results demonstrated that the polymers could fix fractures during the treatment of metaphyseal comminuted fractures in rabbit femurs.

Chen et al.[144] fabricated membranes for drug release using coaxial electrospinning and extrusion-based 3D printing. The membranes consisted of 3D-printed polycaprolactone meshes along with drugs and connective tissue growth factor-loaded poly(lactic-*co*-glycolic acid) electrospun nanofibers. The prepared scaffold imitated the ECM morphology of the connective tissues. The drug-release profile and mechanical strength of the prolapsed membrane were assessed and compared with those of commercially available polypropylene mesh. These studies conclude that the fabricated scaffold had a mechanical strength comparable to that of polypropylene meshes and exhibited sustainable delivery of estradiol for 30 days, lidocaine for 25 days, and metronidazole for 4 days, as confirmed by *in vitro* drug-release tests. Simultaneously, the animal tests revealed that the mechanical strength of the polycaprolactone mesh decreased with time, owing to polymer degradation following implantation. Additionally, the histological images revealed that the composites had no adverse effects.

According to the currently available literature, 3D printing of composite nanofibers is an important strategy that should be widely adopted for engineering advanced medical devices intended for smart drug delivery materials because it offers a way to control the structural and functional characteristics of the material, which ultimately determines how well these systems release drugs. However, because 3D-printed controlled drug delivery systems are theoretically novel, additional studies and clinical trials are required before these materials can be used in practical applications.

4.2.4. 3D-Printed Nanofibers Composites for Medical Devices. The design and engineering of other medical materials using 3D printing have also been explored by

https://doi.org/10.1021/acsomega.3c03920
ACS Omega 2023, 8, 28002−28025

Table 6. 3D-Printed Coelectrospun Materials and Their Biomedical Applications

Material	Applications	ref
3D-printed PCL scaffolds infused with the dispersion of PCL/gelatin nanofibers	Bone tissue engineering	116
3D-printed PLA forming intervertebral disc frame and poly(L-lactide)/octa-armed polyhedral oligomeric silsesquioxanes fibers forming annulus fibrosus structure	Bone tissue engineering	120
Double-layered scaffold consisting of electrospun PCL/gelatin nanofibrous layer and 3D-printed PCL/gelatin/nanohydroxyapatite (nHA)	Bone tissue engineering	121
PLA microstruts and electrospun gelatin-forsterite nanofiber	Bone tissue engineering	148
Gelatin nanofibers/3D-printed PLLA	Subchondral bone-and-nasal-cartilage regeneration	149
3D-printed PLA screw implants coated with electrospun PVA-nHA nanofibers	Bone tissue engineering	112
3D-printed PCL having nanofibers	Bone tissue engineering	123
3D-printed PCL/PLLA nanofibrous composite	Bone tissue engineering	124
3D printing of calcium phosphate pastes with dispersed PLGA nanofiber	Bone tissue engineering	150
3D-printed rabbit tibia made of PCL, covered with electrospun PCL, and grafted with gelatin	Bone tissue regeneration	151
Pamidronate incorporated layered double hydroxides (LDH)/electrospun PCL nanofibers glued with 3D-printed PCL grids	Bone tissue regeneration	152
3D-printed PCL/collagen struts loaded with alginate electrospun nanofibers	Muscle tissue engineering	125
Skeletal structure with 3D-printed frame and PCL/collagen nanofibers implanted within frames	Musculoskeletal tissue regeneration	153
EHD jet-printed PCL filament/dip-coated gelatin hydrogels/PCL nanofibers	Nerve tissue engineering	126
Electrospun PLCL nanofibers grafted with 3D-printed collagen hydrogels	Nerve tissue engineering	114
3D-printed nerve guide made of PCL from an electrospun mat comprising gelatin-poly(3-hydroxybutyrate-*co*-3-hydroxyvalerate)	Nerve tissue engineering	127
3D electrospun scaffolds PLCL and PLGA	Nerve tissue engineering	154
3D-printed PCL framework injected with PLGA nanofibers incorporated hydroxybutyl chitosan hydrogels	Cartilage tissue engineering	129
3D-printed PLA scaffolds coated with PVA/hyaluronic acid nanofibers	Cartilage tissue engineering	130
3D scaffolds from ink consisting of gelatin/PLGA nanofibers blended with CDM and hyaluronic acid	Cartilage tissue engineering	131
3D-printed tracheal constructs consisting of dispersed poly(L-lactide)/gelatin short nanofibers	Tracheal regeneration	132
3D-printed TPU skeletons enveloped with PLA electrospun nanofibers	Tracheal regeneration	133
PCL electrospun nanofibers coated 3D-printed PCL scaffold	Vascular grafts	155
3D-printed blood vessels comprised of chitosan/PCL electrospun nanofibers coated with strands of PCL	Vascular grafts	135
Double-layered vascular construct consisting of luminal polydioxanone (PDO) and an abluminal layer of PCL/PDO + dipyridamole with a 3D-printed PCL spiral filament	Vascular tissue engineering	156
Triple PCL graft by combining E-jet 3D printing, electrospinning, and coelectrospraying	Vascular grafts	157
PLA/gelatin nanofibrous scaffolds by 3D printing using a hand-held electrospinning apparatus	Skin tissue regeneration	137
Electrospun PCL/silk sericin nanofibers and 3D-printed chitosan/sodium alginate hydrogel	Skin tissue regeneration	138
PCL/keratin electrospun scaffold with 3D-printed supporting structure	Multilayered skin substitute	158
Electrospun poly(glycolic acid)/PEG loaded with 3D-printed PVA as a sacrificial element	Wound healing	159
3D-printed PCL covered with electrospun PLGA	Cell therapy and tissue engineering	156
3D-printed PDMS sheets with poly(vinylidene fluoride trifluoroethylene) electrospun nanofibrous mats	Sensor	139
PEO/PCL coaxial nanofibers coated on 3D-printed PLA structure	Tissue engineering and drug delivery	141
3D-printed polylactide cages and drug-loaded nanofibers	Tissue engineering and drug delivery	142
3D-printed polylactide cages and antibiotic-incorporated poly(D,L)-lactide-*co*-glycolide nanofiber	Tissue engineering and drug delivery	143
3D-printed PCL meshes along with drugs and connective tissue growth-factor-loaded PLGA electrospun nanofibers	Drug delivery	144
Electrospun PCL nanofibers supported on 3D-printed PLA frames	Bionic engineered cardiac tissue for tracking electrophysiological activity	145
3D-printed hemodialysis membrane consisting of poly(methyl methacrylate)-*graft*-poly(dimethylsiloxane) nanofibers and polyamide6 nanofibers	Portable hemodialyzer	146
PLA struts were 3D-printed on PLA nanofibers	Masks	147

researchers in recent decades. Accordingly, Wei et al.[145] designed a bionic engineered cardiac tissue (ECT) whose electrophysiology could be tracked by a biosensor coupled with microelectrode arrays (MEAs). ECT was performed by culturing rat cardiomyocytes. The scaffold was composed of 3D-printed PLA frames that acted as a support for the electrospun PCL nanofibers. Mechanical whipping and cell viability tests confirmed the biocompatibility and strength of the ECT. Subsequently, an electrophysiological test was conducted by coupling the MEA sensors with the ECT. The administration of isoprenaline helped check the functioning of the ECT. The system presented by the authors is one of several examples of the utilization of 3D printing and electrospinning as efficient approaches for the preparation of advanced functional medical devices.

Koh and Lee[146] used a 3D printer to design a portable hemodialyzer with an embossed structure. The hemodialysis membrane consisted of poly(methyl methacrylate)-*graft*-poly(dimethylsiloxane) nanofibers having a diameter of 0.437 μm and polyamide6 (PA6) nanofibers having a diameter of 0.072 μm. Further modification of the nanofibrous membrane was performed to enhance the dialysis capability. Negatively charged hemodialysis membranes were formed because of cross-linking and esterification. −OH, the functional groups of poly(ethylene glycol), and the COOH groups of sodium alginate undergo esterification, thereby resulting in membranes with an anionic surface. This may lead to the repulsion

https://doi.org/10.1021/acsomega.3c03920
ACS Omega 2023, 8, 28002−28025

between anionic blood cells and membranes. Additionally, the membranes exhibited hydrophilicity and an enhanced fouling resistance. Moreover, the use of beta-zeolite enhanced the efficiency of the membrane in eradicating creatinine. The dialysis membrane presented here is a proven example of a combination of 3D spinning and electrospinning approaches for the fabrication of functional membranes that could be beneficial for patients with kidney failure, requiring dialysis.

He et al.[147] postulated the fabrication of biodegradable and changeable masks through a combination of 3D printing and electrospinning. The PLA struts were 3D printed onto PLA nanofibers to produce transparent masks. An advantage of their mask was that it was transparent, thus overcoming the threatening appearance of conventional mask materials, which was identified during the COVID-19 pandemic. Their study demonstrated the vital influence of the fabricated material morphology on the filtration performance of the hybrid mask owing to the presence of nanofibers. The mask was flexible and fitted well to the face by using 3D printing.

We believe that the adoption of 3D printing, as presented in the literature and summarized in Table 6, is proof that advanced medical devices can be fabricated with special features that may not be possible by using conventional approaches.

5. CONCLUSIONS AND OUTLOOK

3D printing and electrospinning have both evolved and are highly beneficial in the field of biomedical applications; however, each technique has shortcomings. For instance, 3D printing has a low print resolution, thus resulting in scaffolds with large pores for the adherence of most cells. By contrast, although electrospun scaffolds have high porosity, their pore dimensions are sufficiently small for cell migration and infiltration. The combined approach of 3D printing and electrospinning results in the fabrication of scaffolds with features better than those manufactured using any one of these techniques. Thus, this review focuses on the biomedical applications of the hybrid method.

As this combined approach involves the use of separate hardware for 3D printing and electrospinning, users often have to reposition the sample from one apparatus to another, which may contaminate the sample or cause positioning defects. Positioning slots are particularly significant in 3D printers when electrospinning and 3D printing are used alternatively to ensure the correct alignment of one layer over another. Note that repeated manual positioning does not ensure precision. Thus, developing a platform that combines both techniques will ensure precision and enhance the efficiency of the fabrication technique. In addition, the combined approach can be extended to fabricate materials comprising polymers other than the most commonly used polymer, PCL. This will widen the field of application and increase the choice of raw materials for the fabrication of products for biomedical applications. Most of the research conducted to date has focused on the development of materials for tissue regeneration. The applicability of products synthesized by 3D printing−coelectrospinning can be examined for biosensing, drug delivery, and the fabrication of medical products and masks.

Although this combination approach has a few drawbacks that limit its use in the preclinical and clinical stages, significant research in this field can ensure its use in clinical applications in the future.

AUTHOR INFORMATION

Corresponding Author

Suprakas Sinha Ray − *Centre for Nanostructures and Advanced Materials, DSI-CSIR Nanotechnology Innovation Centre, Council for Scientific and Industrial Research, Pretoria 0001, South Africa; Department of Chemical Sciences, University of Johannesburg, Doorfontein, Johannesburg 2028, South Africa;* orcid.org/0000-0002-0007-2595; Email: rsuprakas@csir.co.za, ssinharay@uj.ac.za

Authors

Adrija Ghosh − *Department of Polymer Science and Technology, University of Calcutta, Kolkata 700009, India*

Jonathan Tersur Orasugh − *Centre for Nanostructures and Advanced Materials, DSI-CSIR Nanotechnology Innovation Centre, Council for Scientific and Industrial Research, Pretoria 0001, South Africa; Department of Chemical Sciences, University of Johannesburg, Doorfontein, Johannesburg 2028, South Africa*

Dipankar Chattopadhyay − *Department of Polymer Science and Technology, University of Calcutta, Kolkata 700009, India; Center for Research in Nanoscience and Nanotechnology, Acharya Prafulla Chandra Roy Sikhsha Prangan, University of Calcutta, Kolkata 700098, India;* orcid.org/0000-0001-9120-8541

Complete contact information is available at: https://pubs.acs.org/10.1021/acsomega.3c03920

Notes

The authors declare no competing financial interest.

ACKNOWLEDGMENTS

The authors would like to thank the Department of Science Innovation (C6ACH35), the Council for Scientific and Industrial Research (086ADMI), and the University of Johannesburg (086310) for their financial support.

REFERENCES

(1) Ventola, C. L. Medical applications for 3D printing: Current and projected uses. *Pharm. Ther.* **2014**, *39* (10), 704.

(2) Saptarshi, S. M.; Zhou, C. Basics of 3D printing: Engineering aspects. In *3D Printing in Orthopaedic Surgery*; Elsevier, 2019; pp 17−30. Starosolski, Z. A.; Kan, J. H.; Rosenfeld, S. D.; Krishnamurthy, R.; Annapragada, A. Application of 3-D printing (rapid prototyping) for creating physical models of pediatric orthopedic disorders. *Pediatr. Radiol.* **2014**, *44* (2), 216−221.

(3) Murr, L. E. Frontiers of 3D printing/additive manufacturing: from human organs to aircraft fabrication. *J. Mater. Sci. Technol.* **2016**, *32* (10), 987−995.

(4) (a) Gokhare, V. G.; Raut, D.; Shinde, D. A review paper on 3D-printing aspects and various processes used in the 3D-printing. *Int. J. Eng. Res. Technol.* **2017**, *6* (06), 953−958. (b) Pîrjan, A.; Petrosanu, D.-M. The impact of 3D printing technology on the society and economy. *J. Infor. Sys. Oper. Man.* **2013**, *7* (2), 360−370.

(5) (a) Hurst, E. J. 3D printing in healthcare: emerging applications. *J. Hosp. Librariansh.* **2016**, *16* (3), 255−267. (b) Matias, E.; Rao, B. 3D printing: On its historical evolution and the implications for business. In *2015 Portland International Conference on Management of Engineering and Technology (PICMET)*; IEEE, 2015; pp 551−558.

(6) (a) Min, J. K.; Mosadegh, B.; Dunham, S.; Al'Aref, S. J. *3D Printing applications in cardiovascular medicine*; Academic Press, 2018. Ali, A.; Ahmad, U.; Akhtar, J. 3D printing in pharmaceutical sector: an overview. *Pharmaceutical Formulation Design-Recent Practices* **2020**, DOI: 10.5772/intechopen.90738. (b) Xu, C.; Liang, J.; Yang, J.

History of Cardiovascular 3D Printing. In *Cardiovascular 3D Printing*; Springer, 2021; pp 1−2.
(7) (a) Groth, C.; Kravitz, N. D.; Jones, P. E.; Graham, J. W.; Redmond, W. R. Three-dimensional printing technology. *J. Clin Orthod* **2014**, *48* (8), 475−485. (b) Gross, B. C.; Erkal, J. L.; Lockwood, S. Y.; Chen, C.; Spence, D. M. Evaluation of 3D printing and its potential impact on biotechnology and the chemical sciences. *Anal. Chem.* **2014**, *86*, 3240−3253.
(8) Sultan, S.; Siqueira, G.; Zimmermann, T.; Mathew, A. P. 3D printing of nano-cellulosic biomaterials for medical applications. *Curr. Opin. Biomed. Eng.* **2017**, *2*, 29−34.
(9) Christensen, R. K.; von Halling Laier, C.; Kiziltay, A.; Wilson, S.; Larsen, N. B. 3D printed hydrogel multiassay platforms for robust generation of engineered contractile tissues. *Biomacromolecules* **2020**, *21* (2), 356−365.
(10) Ackland, D.; Robinson, D.; Lee, P. V. S.; Dimitroulis, G. Design and clinical outcome of a novel 3D-printed prosthetic joint replacement for the human temporomandibular joint. *Cli. Biomech.* **2018**, *56*, 52−60.
(11) Xu, X.; Goyanes, A.; Trenfield, S. J.; Diaz-Gomez, L.; Alvarez-Lorenzo, C.; Gaisford, S.; Basit, A. W. Stereolithography (SLA) 3D printing of a bladder device for intravesical drug delivery. *Mater. Sci. Eng.* **2021**, *120*, 111773.
(12) Silva, V. A.; Fernandes-Junior, W. S.; Rocha, D. P.; Stefano, J. S.; Munoz, R. A.; Bonacin, J. A.; Janegitz, B. C. 3D-printed reduced graphene oxide/polylactic acid electrodes: A new prototyped platform for sensing and biosensing applications. *Biosens. Bioelectron.* **2020**, *170*, 112684.
(13) Elbadawi, M.; McCoubrey, L. E.; Gavins, F. K.; Ong, J. J.; Goyanes, A.; Gaisford, S.; Basit, A. W. Harnessing artificial intelligence for the next generation of 3D printed medicines. *Adv. Drug Delivery Rev.* **2021**, *175*, 113805.
(14) Tucker, N.; Stanger, J. J.; Staiger, M. P.; Razzaq, H.; Hofman, K. The history of the science and technology of electrospinning from 1600 to 1995. *J. Eng. Fibers Fabr.* **2012**, *7*, 63−73.
(15) Kny, E.; Ghosal, K.; Thomas, S. *Electrospinning: From basic research to commercialization*; Royal Society of Chemistry, 2018.
(16) Mirjalili, M.; Zohoori, S. Review for application of electrospinning and electrospun nanofibers technology in textile industry. *J. Nanostruct. Chem.* **2016**, *6* (3), 207−213.
(17) Samanta, A. P.; Ali, M. S.; Orasugh, J. T.; Ghosh, S. K.; Chattopadhyay, D. Crosslinked nanocollagen-cellulose nanofibrils reinforced electrospun polyvinyl alcohol/methylcellulose/polyethylene glycol bionanocomposites: Study of material properties and sustained release of ketorolac tromethamine. *Carbohydr. Polym. Technol. Appl.* **2022**, *3*, 100195.
(18) Yang, D.-L.; Faraz, F.; Wang, J.-X.; Radacsi, N. Combination of 3D Printing and Electrospinning Techniques for Biofabrication. *Adv. Mater. Technol.* **2022**, *7* (7), 2101309.
(19) Pugliese, R.; Beltrami, B.; Regondi, S.; Lunetta, C. Polymeric biomaterials for 3D printing in medicine: An overview. *Annals 3D Print. Med.* **2021**, *2*, 100011.
(20) Bootsma, K.; Fitzgerald, M. M.; Free, B.; Dimbath, E.; Conjerti, J.; Reese, G.; Konkolewicz, D.; Berberich, J. A.; Sparks, J. L. 3D printing of an interpenetrating network hydrogel material with tunable viscoelastic properties. *J. Mech.Beh. Biomed. Mater.* **2017**, *70*, 84−94.
(21) Kumar, S. Synthetic polymers derived single-network inks/bioinks for extrusion-based 3D printing towards bioapplications. *Mater. Adv.* **2021**, *2*, 6928−6941.
(22) (a) Jayaramudu, J.; Reddy, G. S. M.; Varaprasad, K.; Sadiku, E.R.; Sinha Ray, S.; Varada Rajulu, A. Preparation and properties of biodegradable films from Sterculia urens short fiber/cellulose green composites. *Carbohydr. Polym.* **2013**, *93* (2), 622. (b) Wang, J.; Chiappone, A.; Roppolo, I.; Shao, F.; Fantino, E.; Lorusso, M.; Rentsch, D.; Dietliker, K.; Pirri, C. F.; Grützmacher, H. All-in-one cellulose nanocrystals for 3D printing of nanocomposite hydrogels. *Angew. Chem., Int. Ed.* **2018**, *57* (9), 2353−2356.
(23) Cheng, Y.; Qin, H.; Acevedo, N. C.; Jiang, X.; Shi, X. 3D printing of extended-release tablets of theophylline using hydroxypropyl methylcellulose (HPMC) hydrogels. *Int. J. Pharm.* **2020**, *591*, 119983.
(24) Karakurt, I.; Aydogdu, A.; Çıkrıkcı, S.; Orozco, J.; Lin, L. Stereolithography (SLA) 3D printing of ascorbic acid loaded hydrogels: A controlled release study. *Int. J. Pharm.* **2020**, *584*, 119428.
(25) Gutierrez, E.; Burdiles, P. A.; Quero, F.; Palma, P.; Olate-Moya, F.; Palza, H. 3D Printing of Antimicrobial Alginate/Bacterial-Cellulose Composite Hydrogels by Incorporating Copper Nanostructures. *ACS Biomater. Sci. Eng.* **2019**, *5* (11), 6290−6299.
(26) Wu, Z.; Hong, Y. Combination of the Silver−Ethylene Interaction and 3D Printing To Develop Antibacterial Superporous Hydrogels for Wound Management. *ACS Appl. Mater. Interfaces* **2019**, *11* (37), 33734−33747.
(27) Meng, Y.; Cao, J.; Chen, Y.; Yu, Y.; Ye, L. 3D printing of a poly (vinyl alcohol)-based nano-composite hydrogel as an artificial cartilage replacement and the improvement mechanism of printing accuracy. *J. Mater. Chem. B* **2020**, *8* (4), 677−690.
(28) Long, J.; Etxeberria, A. E.; Nand, A. V.; Bunt, C. R.; Ray, S.; Seyfoddin, A. A 3D printed chitosan-pectin hydrogel wound dressing for lidocaine hydrochloride delivery. *Mater. Sci. Eng., C* **2019**, *104*, 109873.
(29) Guo, Z.; Xia, J.; Mi, S.; Sun, W. Mussel-Inspired Naturally Derived Double-Network Hydrogels and Their Application in 3D Printing: From Soft, Injectable Bioadhesives to Mechanically Strong Hydrogels. *ACS Biomater. Sci. Eng.* **2020**, *6* (3), 1798−1808.
(30) Monavari, M.; Homaeigohar, S.; Fuentes-Chandía, M.; Nawaz, Q.; Monavari, M.; Venkatraman, A.; Boccaccini, A. R. 3D printing of alginate dialdehyde-gelatin (ADA-GEL) hydrogels incorporating phytotherapeutic icariin loaded mesoporous SiO2-CaO nanoparticles for bone tissue engineering. *Mater. Sci. Eng.* **2021**, *131*, 112470.
(31) Nosrati, H.; Sarraf Mamoory, R.; Svend Le, D. Q.; Bünger, C. E. Fabrication of gelatin/hydroxyapatite/3D-graphene scaffolds by a hydrogel 3D-printing method. *Mater. Chem. Phys.* **2020**, *239*, 122305.
(32) Jiang, P.; Lin, P.; Yang, C.; Qin, H.; Wang, X.; Zhou, F. 3D printing of dual-physical cross-linking hydrogel with ultrahigh strength and toughness. *Chem. Mater.* **2020**, *32* (23), 9983−9995.
(33) Li, Q.; Xu, S.; Feng, Q.; Dai, Q.; Yao, L.; Zhang, Y.; Gao, H.; Dong, H.; Chen, D.; Cao, X. 3D printed silk-gelatin hydrogel scaffold with different porous structure and cell seeding strategy for cartilage regeneration. *Bioact. Mater.* **2021**, *6* (10), 3396−3410.
(34) Hong, H.; Seo, Y. B.; Kim, D. Y.; Lee, J. S.; Lee, Y. J.; Lee, H.; Ajiteru, O.; Sultan, M. T.; Lee, O. J.; Kim, S. H.; et al. Digital light processing 3D printed silk fibroin hydrogel for cartilage tissue engineering. *Biomaterials* **2020**, *232*, 119679.
(35) Do, A.-V.; Khorsand, B.; Geary, S. M.; Salem, A. K. 3D Printing of Scaffolds for Tissue Regeneration Applications. *Adv. Healthcare Mater.* **2015**, *4* (12), 1742−1762.
(36) Cao, Y.; Xu, X.; Qin, Z.; He, C.; Yan, L.; Hou, F.; Liu, J.; Guo, A. Vat photopolymerization 3D printing of thermal insulating mullite fiber-based porous ceramics. *Addit. Manuf.* **2022**, *60*, 103235.
(37) Mei, H.; Tan, Y.; Huang, W.; Chang, P.; Fan, Y.; Cheng, L. Structure design influencing the mechanical performance of 3D printing porous ceramics. *Ceram. Int.* **2021**, *47* (6), 8389−8397.
(38) Liu, S.; Mo, L.; Bi, G.; Chen, S.; Yan, D.; Yang, J.; Jia, Y.-G.; Ren, L. DLP 3D printing porous β-tricalcium phosphate scaffold by the use of acrylate/ceramic composite slurry. *Ceram. Int.* **2021**, *47* (15), 21108−21116.
(39) Hall, S. E.; Regis, J. E.; Renteria, A.; Chavez, L. A.; Delfín, L.; Vargas, S.; Haberman, M. R.; Espalin, D.; Wicker, R.; Lin, Y. Paste extrusion 3D printing and characterization of lead zirconate titanate piezoelectric ceramics. *Ceram. Int.* **2021**, *47* (15), 22042−22048.
(40) Yang, J.; Yu, R.; Li, X.; He, Y.; Wang, L.; Huang, W.; Jiao, J. Silicon carbide whiskers reinforced SiOC ceramics through digital light processing 3D printing technology. *Ceram. Int.* **2021**, *47* (13), 18314−18322.
(41) Lu, J.; Dong, P.; Zhao, Y.; Zhao, Y.; Zeng, Y. 3D printing of TPMS structural ZnO ceramics with good mechanical properties. *Ceram. Int.* **2021**, *47* (9), 12897−12905.

https://doi.org/10.1021/acsomega.3c03920
ACS Omega 2023, 8, 28002−28025

(42) Carloni, D.; Zhang, G.; Wu, Y. Transparent alumina ceramics fabricated by 3D printing and vacuum sintering. *J. Europ. Ceram. Soc.* **2021**, *41* (1), 781−791.
(43) Zheng, K.; Ding, D.; Quan, Y.; Zhuang, J.; Fei, C.; Zhao, J.; Wang, L.; Zhao, T.; Wang, Z.; Liu, M. 3D printing orientation controlled PMN-PT piezoelectric ceramics. *J. Europ. Cer. Soc.* **2023**, *43*, 2408.
(44) Li, B.; Xue, Z.; Jiang, B.; Feng, T.; Zhang, L.; Wang, X.; He, J. 3D printing of infrared transparent ceramics via material extrusion. *Addit. Man.* **2023**, *61*, 103364.
(45) Huang, Z.; Liu, L. Y.; Yuan, J.; Guo, H.; Wang, H.; Ye, P.; Du, Z.; Zhao, Y.; Zhang, H.; Gan, C. L. Stereolithography 3D printing of Si_3N_4 cellular ceramics with ultrahigh strength by using highly viscous paste. *Ceram. Int.* **2023**, *49* (4), 6984−6995.
(46) Zhang, L.; Liu, H.; Yao, H.; Zeng, Y.; Chen, J. 3D printing of hollow lattice structures of ZrO2(3Y)/Al2O3 ceramics by vat photopolymerization: Process optimization, microstructure evolution and mechanical properties. *J. Man. Proc.* **2022**, *83*, 756−767.
(47) Yu, S.; Zeng, T.; Yang, Y.; Jiang, H.; Wu, R.; Fan, M.; Cheng, S. Effect of an annealing treatment on the microstructure and EMW-absorbing properties of SiCw/Si_3N_4 ceramics fabricated by 3D printing. *Ceram. Int.* **2023**, *49* (1), 1092−1101.
(48) Su, F.; Su, Z.; Liu, Y.; Lin, X.; Cao, J.; Liu, Z.; Wang, P.; Liu, C.; Chen, Z. Generative shaping and material-forming (GSM) enables structure engineering of complex-shaped Li4SiO4 ceramics based on 3D printing of ceramic/polymer precursors. *Addit. Man.* **2022**, *57*, 102963.
(49) Weng, Z.; Zhou, Y.; Lin, W.; Senthil, T.; Wu, L. Structure-property relationship of nano enhanced stereolithography resin for desktop SLA 3D printer. *Composites, Part A* **2016**, *88*, 234−242.
(50) Kholghi Eshkalak, S.; Kowsari, E.; Ramakrishna, S. 17 - 3D printing of graphene-based composites and their applications in medicine and health care. In *Innovations in Graphene-Based Polymer Composites*; Rangappa, S. M., Parameswaranpillai, J., Ayyappan, V., Motappa, M. G., Siengchin, S., Soutis, C., Eds.; Woodhead Publishing, 2022; pp 463−485.
(51) Lee, E.-D.; Sim, J.-H.; Kweon, H.-J.; Paik, I.-H. Determination of process parameters in stereolithography using neural network. *KSME Int. J.* **2004**, *18* (3), 443−452.
(52) Chockalingam, K.; Jawahar, N.; Ramanathan, K. N.; Banerjee, P. S. Optimization of stereolithography process parameters for part strength using design of experiments. *Int. J. Adv. Man. Technol.* **2006**, *29* (1), 79−88.
(53) (a) Kundu, A.; Shetti, N. P.; Basu, S.; Mondal, K.; Sharma, A.; Aminabhavi, T. M. Versatile carbon nanofiber-based sensors. *ACS Appl. Bio Mater.* **2022**, *5* (9), 4086−4102. (b) Bettinger, C. J.; Borenstein, J. T.; Langer, R. Micro-and nanofabricated scaffolds. In *Principles of Tissue Engineering*; Elsevier, 2007; pp 341−358.
(54) Sola, A.; Trinchi, A. Chapter 2 - Basic principles of fused deposition modeling. In *Fused Deposition Modeling of Composite Materials*; Sola, A., Trinchi, A., Eds.; Woodhead Publishing, 2023; pp 7−39.
(55) Manoj Prabhakar, M.; Saravanan, A.; Haiter Lenin, A.; Jerin leno, I.; Mayandi, K.; Sethu Ramalingam, P. A short review on 3D printing methods, process parameters and materials. *Mater. Today: Proceedings* **2021**, *45*, 6108.
(56) (a) Riza, S.; Masood, S.; Wen, C. Laser-assisted additive manufacturing for metallic biomedical scaffolds. *Comprehensive Materials Processing* **2014**, *10*, 285−301. (b) Munir, K. S.; Li, Y.; Wen, C. Metallic scaffolds manufactured by selective laser melting for biomedical applications. In *Metallic Foam Bone*; Elsevier, 2017; pp 1−23.
(57) Ruban, W.; Vijayakumar, V.; Dhanabal, P.; Pridhar, T. Effective process parameters in selective laser sintering. *Int. J. Rapid Man.* **2014**, *4* (2−4), 148−164.
(58) Singh, S.; Sachdeva, A.; Sharma, V. S. Optimization of selective laser sintering process parameters to achieve the maximum density and hardness in polyamide parts. *Prog. Addit. Man.* **2017**, *2* (1), 19−30.
(59) Kumar, S. A.; Prasad, R. Basic principles of additive manufacturing: different additive manufacturing technologies. In *Additive manufacturing*; Elsevier, 2021; pp 17−35.
(60) Ginestra, P.; Rovetta, R.; Fiorentino, A.; Ceretti, E. Bioprinting process optimization: Evaluation of parameters influence on the extrusion of inorganic polymers. *Procedia CIRP* **2020**, *89*, 104−109.
(61) Mazzanti, V.; Malagutti, L.; Mollica, F. FDM 3D printing of polymers containing natural fillers: A review of their mechanical properties. *Polymers* **2019**, *11* (7), 1094.
(62) Shahzad, K.; Deckers, J.; Zhang, Z.; Kruth, J.-P.; Vleugels, J. Additive manufacturing of zirconia parts by indirect selective laser sintering. *J. Eur. Ceram. Soc.* **2014**, *34* (1), 81−89.
(63) Ahn, D.; Kweon, J.-H.; Choi, J.; Lee, S. Quantification of surface roughness of parts processed by laminated object manufacturing. *J. Mater. Process. Technol.* **2012**, *212* (2), 339−346.
(64) Lovecchio, J.; Cortesi, M.; Zani, M.; Govoni, M.; Dallari, D.; Giordano, E. Fiber Thickness and Porosity Control in a Biopolymer Scaffold 3D Printed through a Converted Commercial FDM Device. *Materials* **2022**, *15*, 2394.
(65) Shi, K.; Tan, D. K.; Nokhodchi, A.; Maniruzzaman, M. Drop-on-powder 3D printing of tablets with an anti-cancer drug, 5-fluorouracil. *Pharmaceutics* **2019**, *11* (4), 150.
(66) Gioumouxouzis, C. I.; Baklavaridis, A.; Katsamenis, O. L.; Markopoulou, C. K.; Bouropoulos, N.; Tzetzis, D.; Fatouros, D. G. A 3D printed bilayer oral solid dosage form combining metformin for prolonged and glimepiride for immediate drug delivery. *Eur. J. Pharm. Sci.* **2018**, *120*, 40−52.
(67) Jiang, H.; Yu, X.; Fang, R.; Xiao, Z.; Jin, Y. 3D printed mold-based capsaicin candy for the treatment of oral ulcer. *Int. J. Pharm.* **2019**, *568*, 118517.
(68) Matijašić, G.; Gretić, M.; Vinčić, J.; Poropat, A.; Cuculić, L.; Rahelić, T. Design and 3D printing of multi-compartmental PVA capsules for drug delivery. *J. Drug Delivery Sci. Technol.* **2019**, *52*, 677−686.
(69) Khosraviboroujeni, A.; Mirdamadian, S. Z.; Minaiyan, M.; Taheri, A. Preparation and characterization of 3D printed PLA microneedle arrays for prolonged transdermal drug delivery of estradiol valerate. *Drug Delivery Transl. Res.* **2022**, *12* (5), 1195−1208.
(70) Kim, D.; Kim, H.; Lee, P. C.; Lee, J. B. Universally applicable RNA membrane-based microneedle system for transdermal drug delivery. *Mater. Horiz.* **2020**, *7* (5), 1317−1326.
(71) Cox, S. C.; Thornby, J. A.; Gibbons, G. J.; Williams, M. A.; Mallick, K. K. 3D printing of porous hydroxyapatite scaffolds intended for use in bone tissue engineering applications. *Mater. Sci. Eng., C* **2015**, *47*, 237−247.
(72) Kabirian, F.; Ditkowski, B.; Zamanian, A.; Heying, R.; Mozafari, M. An innovative approach towards 3D-printed scaffolds for the next generation of tissue-engineered vascular grafts. *Mater. Today: Proc.* **2018**, *5* (7), 15586−15594.
(73) Huang, L.; Gao, J.; Wang, H.; Xia, B.; Yang, Y.; Xu, F.; Zheng, X.; Huang, J.; Luo, Z. Fabrication of 3D scaffolds displaying biochemical gradients along longitudinally oriented microchannels for neural tissue engineering. *ACS Appl. Mater. Interfaces* **2020**, *12* (43), 48380−48394.
(74) You, F.; Wu, X.; Zhu, N.; Lei, M.; Eames, B. F.; Chen, X. 3D printing of porous cell-laden hydrogel constructs for potential applications in cartilage tissue engineering. *ACS Biomater. Sci. Eng.* **2016**, *2* (7), 1200−1210.
(75) Rhee, S.; Puetzer, J. L.; Mason, B. N.; Reinhart-King, C. A.; Bonassar, L. J. 3D bioprinting of spatially heterogeneous collagen constructs for cartilage tissue engineering. *ACS Biomater. Sci. Eng.* **2016**, *2* (10), 1800−1805.
(76) Xiang, D.; Zhang, X.; Han, Z.; Zhang, Z.; Zhou, Z.; Harkin-Jones, E.; Zhang, J.; Luo, X.; Wang, P.; Zhao, C.; Li, Y. 3D printed high-performance flexible strain sensors based on carbon nanotube and graphene nanoplatelet filled polymer composites. *J. Mater. Sci.* **2020**, *55* (33), 15769−15786.
(77) Damiati, S.; Küpcü, S.; Peacock, M.; Eilenberger, C.; Zamzami, M.; Qadri, I.; Choudhry, H.; Sleytr, U. B.; Schuster, B. Acoustic and

https://doi.org/10.1021/acsomega.3c03920
ACS Omega 2023, 8, 28002−28025

hybrid 3D-printed electrochemical biosensors for the real-time immunodetection of liver cancer cells (HepG2). *Biosens. Bioelectron.* **2017**, *94*, 500−506.
(78) Cardoso, R. M.; Silva, P. R.; Lima, A. P.; Rocha, D. P.; Oliveira, T. C.; do Prado, T. M.; Fava, E. L.; Fatibello-Filho, O.; Richter, E. M.; Munoz, R. A. 3D-Printed graphene/polylactic acid electrode for bioanalysis: Biosensing of glucose and simultaneous determination of uric acid and nitrite in biological fluids. *Sens. Actuators, B* **2020**, *307*, 127621.
(79) Geng, X.; Kwon, O.H.; Jang, J. Electrospinning of chitosan dissolved in concentrated acetic acid solution. *Biomaterials* **2005**, *26*, 5427−5432.
(80) Haider, S.; Park, S.-Y. Preparation of the electrospun chitosan nanofibers and their applications to the adsorption of Cu (II) and Pb (II) ions from an aqueous solution. *J. Membr. Sci.* **2009**, *328* (1−2), 90−96.
(81) Rho, K. S.; Jeong, L.; Lee, G.; Seo, B.-M.; Park, Y. J.; Hong, S.-D.; Roh, S.; Cho, J. J.; Park, W. H.; Min, B.-M. Electrospinning of collagen nanofibers: effects on the behavior of normal human keratinocytes and early-stage wound healing. *Biomaterials* **2006**, *27* (8), 1452−1461.
(82) Ghassemi, Z.; Slaughter, G. Storage stability of electrospun pure gelatin stabilized with EDC/Sulfo-NHS. *Biopolymers* **2018**, *109* (9), No. e23232.
(83) Shekarforoush, E.; Faralli, A.; Ndoni, S.; Mendes, A. C.; Chronakis, I. S. Electrospinning of xanthan polysaccharide. *Macromol. Mater. Eng.* **2017**, *302* (8), 1700067.
(84) Celebioglu, A.; Uyar, T. Cyclodextrin nanofibers by electrospinning. *Chem. Commun.* **2010**, *46* (37), 6903−6905.
(85) Melendez-Rodriguez, B.; Reis, M. A. M.; Carvalheira, M.; Sammon, C.; Cabedo, L.; Torres-Giner, S.; Lagaron, J. M. Development and Characterization of Electrospun Biopapers of Poly (3-hydroxybutyrate-co-3-hydroxyvalerate) Derived from Cheese Whey with Varying 3-Hydroxyvalerate Contents. *Biomacromolecules* **2021**, *22* (7), 2935−2953.
(86) Borisova, I.; Stoilova, O.; Manolova, N.; Rashkov, I. Modulating the mechanical properties of electrospun PHB/PCL materials by using different types of collectors and heat sealing. *Polymers (Basel)* **2020**, *12* (3), 693.
(87) Ghosh, A.; Orasugh, J. T.; Chattopadhyay, D.; Ghosh, S. Electrospun nanofibres: A new vista for detection and degradation of harmful endocrine-disrupting chemicals. *Ground. Sust. Dev.* **2022**, *16*, 100716.
(88) Orasugh, J. T.; Ghosh, S. K.; Chattopadhyay, D. Nanofiber-reinforced biocomposites. In *Fiber-Reinforced Nanocomposites: Fundamentals and Applications*; Elsevier, 2020; pp 199−233.
(89) Dodero, A.; Brunengo, E.; Alloisio, M.; Sionkowska, A.; Vicini, S.; Castellano, M. Chitosan-based electrospun membranes: Effects of solution viscosity, coagulant and crosslinker. *Carbohydr. Polym.* **2020**, *235*, 115976.
(90) Moshfeghian, M.; Azimi, H.; Mahkam, M.; Kalaee, M.; Mazinani, S.; Mosafer, H. Effect of solution properties on electrospinning of polymer nanofibers: A study on fabrication of PVDF nanofibers by electrospinning in DMAC and (DMAC/acetone) solvents. *Adv. Appl. NanoBio-Technol.* **2021**, *2* (2), 53−58.
(91) Zaarour, B.; Zhu, L.; Jin, X. Controlling the surface structure, mechanical properties, crystallinity, and piezoelectric properties of electrospun PVDF nanofibers by maneuvering molecular weight. *Soft Mater.* **2019**, *17* (2), 181−189.
(92) Topuz, F.; Satilmis, B.; Uyar, T. Electrospinning of uniform nanofibers of Polymers of Intrinsic Microporosity (PIM-1): The influence of solution conductivity and relative humidity. *Polymer* **2019**, *178*, 121610.
(93) Liu, Z.; Ju, K.; Wang, Z.; Li, W.; Ke, H.; He, J. Electrospun jets number and nanofiber morphology effected by voltage value: Numerical simulation and experimental verification. *Nanoscale Res. Lett.* **2019**, *14* (1), 310.
(94) Motamedi, A. S.; Mirzadeh, H.; Hajiesmaeilbaigi, F.; Bagheri-Khoulenjani, S.; Shokrgozar, M. Effect of electrospinning parameters on morphological properties of PVDF nanofibrous scaffolds. *Prog. Biomater.* **2017**, *6* (3), 113−123.
(95) Bakar, S.; Fong, K.; Eleyas, A.; Nazeri, M. Effect of voltage and flow rate electrospinning parameters on polyacrylonitrile electrospun fibers. In *IOP Conf. Ser.: Mater. Sci. Eng.* IOP Publishing, 2018; Vol. *318*, p 012076.
(96) Nazari, T.; Garmabi, H. The effects of processing parameters on the morphology of PLA/PEG melt electrospun fibers. *Polym. Int.* **2018**, *67* (2), 178−188.
(97) Halabi, M.; Mann-Lahav, M.; Beilin, V.; Shter, G. E.; Elishav, O.; Grader, G. S.; Dekel, D. R. Electrospun anion-conducting ionomer fibers—effect of humidity on final properties. *Polymers* **2020**, *12* (5), 1020.
(98) Rešček, A.; Katančić, Z.; Kratofil Krehula, L.; Šćetar, M.; Hrnjak-Murgić, Z.; Galić, K. Development of double-layered PE/PCL films for food packaging modified with zeolite and magnetite nanoparticles. *Adv. Polym. Technol.* **2018**, *37* (3), 837−842.
(99) Hong, H.; Zhang, D.; Lin, S.; Han, F.; Wang, K.; Jiang, D.; Wu, J.; Mo, X.; Wang, H. Green electrospun silk fibroin nanofibers loaded with cationic ethosomes for transdermal drug delivery. *Chem. Res. Chin. Univ.* **2021**, *37* (3), 488−495.
(100) Sun, Y.; Wang, Q.; Shi, X.; Li, J.; Yao, Q.; Zhang, P. Fabrication of epirubicin loaded core/shell electrospun fibers with effective transdermal sustained-release properties. *Mater. Lett.* **2021**, *299*, 130117.
(101) Qin, Z.-y.; Jia, X.-W.; Liu, Q.; Kong, B.-h.; Wang, H. Fast dissolving oral films for drug delivery prepared from chitosan/pullulan electrospinning nanofibers. *Int. J. Biol. Macromol.* **2019**, *137*, 224−231.
(102) Nazari, K.; Kontogiannidou, E.; Ahmad, R. H.; Gratsani, A.; Rasekh, M.; Arshad, M. S.; Sunar, B. S.; Armitage, D.; Bouropoulos, N.; Chang, M.-W.; et al. Development and characterisation of cellulose based electrospun mats for buccal delivery of non-steroidal anti-inflammatory drug (NSAID). *Eur. J. Pharm. Sci.* **2017**, *102*, 147−155.
(103) Mishima, K.; Du, X.; Miyamoto, N.; Kano, N.; Imaizumi, H. Experimental and theoretical studies on the adsorption mechanisms of uranium (VI) ions on chitosan. *J. Funct. Biomater.* **2018**, *9* (3), 49.
(104) Sadeghianmaryan, A.; Karimi, Y.; Naghieh, S.; Alizadeh Sardroud, H.; Gorji, M.; Chen, X. Electrospinning of scaffolds from the polycaprolactone/polyurethane composite with graphene oxide for skin tissue engineering. *Appl. Biochem. Biotechnol.* **2020**, *191* (2), 567−578.
(105) Pedram Rad, Z.; Mokhtari, J.; Abbasi, M. Calendula officinalis extract/PCL/Zein/Gum arabic nanofibrous bio-composite scaffolds via suspension, two-nozzle and multilayer electrospinning for skin tissue engineering. *Int. J. Biol. Macromol.* **2019**, *135*, 530−543.
(106) Saudi, A.; Rafienia, M.; Zargar Kharazi, A.; Salehi, H.; Zarrabi, A.; Karevan, M. Design and fabrication of poly (glycerol sebacate)-based fibers for neural tissue engineering: Synthesis, electrospinning, and characterization. *Polym. Adv. Technol.* **2019**, *30* (6), 1427−1440.
(107) Paimard, G.; Shahlaei, M.; Moradipour, P.; Akbari, H.; Jafari, M.; Arkan, E. An Impedimetric Immunosensor modified with electrospun core-shell nanofibers for determination of the carcinoma embryonic antigen. *Sens. Actuators, B* **2020**, *311*, 127928.
(108) Tripathy, S.; Gangwar, R.; Supraja, P.; Rao, A. N.; Vanjari, S. R. K.; Singh, S. G. Graphene doped Mn2O3 nanofibers as a facile electroanalytical DNA point mutation detection platform for early diagnosis of breast/ovarian cancer. *Electroanalysis* **2018**, *30* (9), 2110−2120.
(109) Ismail, I.; Abu Bakar, N. F.; Tan, H. L.; Ideris, N.; Mohd Zain, Z.; Idris, S. S.; Radacsi, N. Ultra-sensitive electrosprayed AuNPs-decorated PAA/PAN electrospun nanofibers as glucose sensor. *J. Mater. Res.* **2021**, *36* (21), 4317−4328.
(110) Rajzer, I.; Kurowska, A.; Jabłoński, A.; Jatteau, S.; Sliwka, M.; Ziabka, M.; Menaszek, E. Layered gelatin/PLLA scaffolds fabricated by electrospinning and 3D printing- for nasal cartilages and subchondral bone reconstruction. *Mater. Des.* **2018**, *155*, 297−306.

https://doi.org/10.1021/acsomega.3c03920
ACS Omega 2023, 8, 28002−28025

(111) Efimov, A.; Agapova, O.; Safonova, L.; Bobrova, M.; Parfenov, V.; Koudan, E.; Pereira, F.; Bulanova, E.; Mironov, V.; Agapov, I. 3D scanning probe nanotomography of tissue spheroid fibroblasts interacting with electrospun polyurethane scaffold. *Express Polym. Lett.* **2019**, *13* (7), 632−641.
(112) Saniei, H.; Mousavi, S. Surface modification of PLA 3D-printed implants by electrospinning with enhanced bioactivity and cell affinity. *Polymer* **2020**, *196*, 122467.
(113) Pensa, N. W.; Curry, A. S.; Bonvallet, P. P.; Bellis, N. F.; Rettig, K. M.; Reddy, M. S.; Eberhardt, A. W.; Bellis, S. L. 3D printed mesh reinforcements enhance the mechanical properties of electrospun scaffolds. *Biomat. Res.* **2019**, *23* (1), 22.
(114) Yoo, J.; Park, J. H.; Kwon, Y. W.; Chung, J. J.; Choi, I. C.; Nam, J. J.; Lee, H. S.; Jeon, E. Y.; Lee, K.; Kim, S. H.; Jung, Y.; Park, J. W. Augmented peripheral nerve regeneration through elastic nerve guidance conduits prepared using a porous PLCL membrane with a 3D printed collagen hydrogel. *Biomat. Sci.* **2020**, *8* (22), 6261−6271.
(115) Kim, G.; Son, J.; Park, S.; Kim, W. Hybrid Process for Fabricating 3D Hierarchical Scaffolds Combining Rapid Prototyping and Electrospinning. *Macromol. Rapid Commun.* **2008**, *29* (19), 1577−1581.
(116) Yu, Y.; Hua, S.; Yang, M.; Fu, Z.; Teng, S.; Niu, K.; Zhao, Q.; Yi, C. Fabrication and characterization of electrospinning/3D printing bone tissue engineering scaffold. *RSC Adv.* **2016**, *6* (112), 110557−110565.
(117) Nonato, R. C.; Mei, L. H. I.; Bonse, B. C.; Chinaglia, E. F.; Morales, A. R. Nanocomposites of PLA containing ZnO nanofibers made by solvent cast 3D printing: Production and characterization. *Eur. Polym. J.* **2019**, *114*, 271−278.
(118) Fazal, F.; Diaz Sanchez, F. J.; Waqas, M.; Koutsos, V.; Callanan, A.; Radacsi, N. A modified 3D printer as a hybrid bioprinting-electrospinning system for use in vascular tissue engineering applications. *Med. Eng. Phys.* **2021**, *94*, 52−60.
(119) Yang, D. L.; Faraz, F.; Wang, J. X.; Radacsi, N. Combination of 3D printing and electrospinning techniques for biofabrication. *Adv. Mater. Technol.* **2022**, *7*, 2101309.
(120) Zhu, M.; Tan, J.; Liu, L.; Tian, J.; Li, L.; Luo, B.; Zhou, C.; Lu, L. Construction of biomimetic artificial intervertebral disc scaffold via 3D printing and electrospinning. *Mater. Sci. Eng.: C* **2021**, *128*, 112310.
(121) Liu, J.; Zou, Q.; Wang, C.; Lin, M.; Li, Y.; Zhang, R.; Li, Y. Electrospinning and 3D printed hybrid bi-layer scaffold for guided bone regeneration. *Mater. Des.* **2021**, *210*, 110047.
(122) Naghieh, S.; Foroozmehr, E.; Badrossamay, M.; Kharaziha, M. Combinational processing of 3D printing and electrospinning of hierarchical poly(lactic acid)/gelatin-forsterite scaffolds as a biocomposite: Mechanical and biological assessment. *Mater. Des.* **2017**, *133*, 128−135.
(123) Huang, B.; Aslan, E.; Jiang, Z.; Daskalakis, E.; Jiao, M.; Aldalbahi, A.; Vyas, C.; Bártolo, P. Engineered dual-scale poly (ε-caprolactone) scaffolds using 3D printing and rotational electrospinning for bone tissue regeneration. *Addit. Manuf.* **2020**, *36*, 101452.
(124) Liu, X.; Chen, M.; Luo, J.; Zhao, H.; Zhou, X.; Gu, Q.; Yang, H.; Zhu, X.; Cui, W.; Shi, Q. Immunopolarization-regulated 3D printed-electrospun fibrous scaffolds for bone regeneration. *Biomaterials* **2021**, *276*, 121037.
(125) Yeo, M.; Kim, G. Micro/nano-hierarchical scaffold fabricated using a cell electrospinning/3D printing process for co-culturing myoblasts and HUVECs to induce myoblast alignment and differentiation. *Acta Biomaterialia* **2020**, *107*, 102−114.
(126) Liu, S.; Sun, L.; Zhang, H.; Hu, Q.; Wang, Y.; Ramalingam, M. High-resolution combinatorial 3D printing of gelatin-based biomimetic triple-layered conduits for nerve tissue engineering. *Int. J. Biol. Macromol.* **2021**, *166*, 1280−1291.
(127) Dursun Usal, T.; Yesiltepe, M.; Yucel, D.; Sara, Y.; Hasirci, V. Fabrication of a 3D printed PCL nerve guide: In vitro and in vivo testing. *Macromol. Biosci.* **2022**, *22* (3), 2100389.
(128) Namhongsa, M.; Daranarong, D.; Sriyai, M.; Molloy, R.; Ross, S.; Ross, G. M.; Tuantranont, A.; Tocharus, J.; Sivasinprasasn, S.; Topham, P. D.; et al. Surface-Modified Polypyrrole-Coated PLCL and PLGA Nerve Guide Conduits Fabricated by 3D Printing and Electrospinning. *Biomacromolecules* **2022**, *23* (11), 4532−4546.
(129) Liu, X.; Song, S.; Huang, J.; Fu, H.; Ning, X.; He, Y.; Zhang, Z. HBC-nanofiber hydrogel scaffolds with 3D printed internal microchannels for enhanced cartilage differentiation. *J. Mater. Chem. B* **2020**, *8* (28), 6115−6127.
(130) Farsi, M.; Asefnejad, A.; Baharifar, H. A hyaluronic acid/PVA electrospun coating on 3D printed PLA scaffold for orthopedic application. *Prog. Biomater.* **2022**, *11* (1), 67−77.
(131) Chen, W.; Xu, Y.; Li, Y.; Jia, L.; Mo, X.; Jiang, G.; Zhou, G. 3D printing electrospinning fiber-reinforced decellularized extracellular matrix for cartilage regeneration. *Chem. Eng. J.* **2020**, *382*, 122986.
(132) Yuan, Z.; Ren, Y.; Shafiq, M.; Chen, Y.; Tang, H.; Li, B.; EL-Newehy, M.; EL-Hamshary, H.; Morsi, Y.; Zheng, H.; Mo, X. Converging 3D printing and electrospinning: effect of poly (L-lactide)/gelatin based short nanofibers aerogels on tracheal regeneration. *Macromol. Biosci.* **2022**, *22* (1), 2100342.
(133) Kang, Y.; Wang, C.; Qiao, Y.; Gu, J.; Zhang, H.; Peijs, T.; Kong, J.; Zhang, G.; Shi, X. Tissue-engineered trachea consisting of electrospun patterned sc-PLA/GO-g-IL fibrous membranes with antibacterial property and 3D-printed skeletons with elasticity. *Biomacromolecules* **2019**, *20* (4), 1765−1776.
(134) Mayoral, I.; Bevilacqua, E.; Gómez, G.; Hmadcha, A.; González-Loscertales, I.; Reina, E.; Sotelo, J.; Domínguez, A.; Pérez-Alcántara, P.; Smani, Y.; et al. Tissue engineered in-vitro vascular patch fabrication using hybrid 3D printing and electrospinning. *Mater. Today Bio* **2022**, *14*, 100252.
(135) Lee, S. J.; Heo, D. N.; Park, J. S.; Kwon, S. K.; Lee, J. H.; Lee, J. H.; Kim, W. D.; Kwon, I. K.; Park, S. A. Characterization and preparation of bio-tubular scaffolds for fabricating artificial vascular grafts by combining electrospinning and a 3D printing system. *Phys. Chem. Chem. Phys.* **2015**, *17* (5), 2996−2999.
(136) Huang, R.; Gao, X.; Wang, J.; Chen, H.; Tong, C.; Tan, Y.; Tan, Z. Triple-Layer Vascular Grafts Fabricated by Combined E-Jet 3D Printing and Electrospinning. *Ann. Biomed. Eng.* **2018**, *46* (9), 1254−1266.
(137) Chen, H.; Zhang, H.; Shen, Y.; Dai, X.; Wang, X.; Deng, K.; Long, X.; Liu, L.; Zhang, X.; Li, Y.; Xu, T. Instant in-situ tissue repair by biodegradable PLA/Gelatin nanofibrous membrane using a 3D printed handheld electrospinning device. *Front. Bioeng. Biotechnol.* **2021**, *9*, 684105.
(138) Miguel, S. P.; Cabral, C. S. D.; Moreira, A. F.; Correia, I. J. Production and characterization of a novel asymmetric 3D printed construct aimed for skin tissue regeneration. *Colloids Surf., B* **2019**, *181*, 994−1003.
(139) Lee, H. B.; Kim, Y. W.; Yoon, J.; Lee, N. K.; Park, S.-H. 3D customized and flexible tactile sensor using a piezoelectric nanofiber mat and sandwich-molded elastomer sheets. *Smart Mater. Struct.* **2017**, *26* (4), 045032.
(140) Chen, T.; Bakhshi, H.; Liu, L.; Ji, J.; Agarwal, S. Combining 3D Printing with Electrospinning for Rapid Response and Enhanced Designability of Hydrogel Actuators. *Adv. Funct. Mater.* **2018**, *28* (19), 1800514.
(141) Dos Santos, D. M.; De Annunzio, S. R.; Carmello, J. C.; Pavarina, A. C.; Fontana, C. R.; Correa, D. S. Combining Coaxial Electrospinning and 3D Printing: Design of Biodegradable Bilayered Membranes with Dual Drug Delivery Capability for Periodontitis Treatment. *ACS Appl. Bio Mater.* **2022**, *5* (1), 146−159.
(142) Chou, P.-Y.; Lee, D.; Chen, S.-H.; Liao, C.-T.; Lo, L.-J.; Liu, S.-J. 3D-printed/electrospun bioresorbable nanofibrous drug-eluting cuboid frames for repair of alveolar bone defects. *Int. J. Pharm.* **2022**, *615*, 121497.
(143) Chou, Y.-C.; Lee, D.; Chang, T.-M.; Hsu, Y.-H.; Yu, Y.-H.; Chan, E.-C.; Liu, S.-J. Combination of a biodegradable three-dimensional (3D)−printed cage for mechanical support and nano-

https://doi.org/10.1021/acsomega.3c03920
ACS Omega 2023, 8, 28002−28025

fibrous membranes for sustainable release of antimicrobial agents for treating the femoral metaphyseal comminuted fracture. *J. Mech. Behav. Biomed. Mater.* **2017**, *72*, 209−218.
(144) Chen, Y.-P.; Lo, T.-S.; Lin, Y.-T.; Chien, Y.-H.; Lu, C.-J.; Liu, S.-J. Fabrication of drug-eluting polycaprolactone/poly (lactic-co-glycolic acid) prolapse mats using solution-extrusion 3D printing and coaxial electrospinning techniques. *Polymers* **2021**, *13* (14), 2295.
(145) Wei, X.; Gao, Q.; Xie, C.; Gu, C.; Liang, T.; Wan, H.; Zhuang, L.; He, Y.; Wang, P. Extracellular recordings of bionic engineered cardiac tissue based on a porous scaffold and microelectrode arrays. *Analyt. Meth.* **2019**, *11* (46), 5872−5879.
(146) Koh, E.; Lee, Y. T. Development of an embossed nanofiber hemodialysis membrane for improving capacity and efficiency via 3D printing and electrospinning technology. *Sep. Purif. Technol.* **2020**, *241*, 116657.
(147) He, H.; Gao, M.; Illés, B.; Molnar, K. 3D Printed and electrospun, transparent, hierarchical polylactic acid mask nanoporous filter. *Int. J. Bioprint* **2020**, *6* (4), 278.
(148) Naghieh, S.; Foroozmehr, E.; Badrossamay, M.; Kharaziha, M. Combinational processing of 3D printing and electrospinning of hierarchical poly(lactic acid)/gelatin-forsterite scaffolds as a bio-composite: Mechanical and biological assessment. *Mater. Des.* **2017**, *133*, 128−135.
(149) Rajzer, I.; Kurowska, A.; Jabłoński, A.; Jatteau, S.; Sliwka, M.; Ziabka, M.; Menaszek, E. Layered gelatin/PLLA scaffolds fabricated by electrospinning and 3D printing-for nasal cartilages and subchondral bone reconstruction. *Mater. Des.* **2018**, *155*, 297−306.
(150) Zhao, G.; Cui, R.; Chen, Y.; Zhou, S.; Wang, C.; Hu, Z.; Zheng, X.; Li, M.; Qu, S. 3D Printing of well dispersed electrospun PLGA fiber toughened calcium phosphate scaffolds for osteoanagenesis. *J. Bionic Eng.* **2020**, *17* (4), 652−668.
(151) Rosales-Ibáñez, R.; Viera-Ruiz, A. E.; Cauich-Rodríguez, J. V.; Carrillo-Escalante, H. J.; González-González, A.; Rodríguez-Martínez, J. J.; Hernández-Sánchez, F. Electrospun/3D-printed PCL bioactive scaffold for bone regeneration. *Polym. Bull.* **2023**, *80*, 2533−2552.
(152) (a) Ray, S. S. *Environmentally Friendly Polymer Nanocomposites: Types, Processing and Properties*; Elsevier: Oxford, UK, 2013; ISBN 9780857097774. (b) Belgheisi, G.; Haghbin Nazarpak, M.; Solati-Hashjin, M. Fabrication and evaluation of combined 3D printed/pamidronate-layered double hydroxides enriched electrospun scaffolds for bone tissue engineering applications. *Appl. Clay Sci.* **2022**, *225*, 106538.
(153) Sooriyaarachchi, D.; Wu, J.; Feng, A.; Islam, M.; Tan, G. Z. Hybrid fabrication of biomimetic meniscus scaffold by 3D printing and parallel electrospinning. *Procedia Man.* **2019**, *34*, 528−534.
(154) Namhongsa, M.; Daranarong, D.; Sriyai, M.; Molloy, R.; Ross, S.; Ross, G. M.; Tuantranont, A.; Tocharus, J.; Sivasinprasasn, S.; Topham, P. D.; et al. Surface-modified polypyrrole-coated PLCL and PLGA nerve guide conduits fabricated by 3D printing and electrospinning. *Biomacromolecules* **2022**, *23* (11), 4532−4546.
(155) Mayoral, I.; Bevilacqua, E.; Gómez, G.; Hmadcha, A.; González-Loscertales, I.; Reina, E.; Sotelo, J.; Domínguez, A.; Pérez-Alcántara, P.; Smani, Y.; et al. Tissue engineered in-vitro vascular patch fabrication using hybrid 3D printing and electrospinning. *Mater. Today Bio* **2022**, *14*, 100252.
(156) Maurmann, N.; Pereira, D. P.; Burguez, D.; de S Pereira, F. D.; Neto, P. I.; Rezende, R. A.; Gamba, D.; da Silva, J. V.; Pranke, P. Mesenchymal stem cells cultivated on scaffolds formed by 3D printed PCL matrices, coated with PLGA electrospun nanofibers for use in tissue engineering. *Biomed. Phys. Eng. Express.* **2017**, *3* (4), 045005.
(157) Huang, R.; Gao, X.; Wang, J.; Chen, H.; Tong, C.; Tan, Y.; Tan, Z. Triple-layer vascular grafts fabricated by combined E-Jet 3D printing and electrospinning. *Ann. Biomed. Eng.* **2018**, *46*, 1254−1266.
(158) Choi, W. S.; Kim, J. H.; Ahn, C. B.; Lee, J. H.; Kim, Y. J.; Son, K. H.; Lee, J. W. Development of a multi-layer skin substitute using human hair keratinic extract-based hybrid 3D printing. *Polymers* **2021**, *13* (16), 2584.
(159) Clohessy, R. M.; Cohen, D. J.; Stumbraite, K.; Boyan, B. D.; Schwartz, Z. In vivo evaluation of an electrospun and 3D printed cellular delivery device for dermal wound healing. *J. Biomed. Mater. Res., Part B* **2020**, *108* (6), 2560−2570.

https://doi.org/10.1021/acsomega.3c03920
ACS Omega 2023, 8, 28002−28025